
# How Does Drifter Position Uncertainty Affect Ocean Dispersion Estimates?

ANGELIQUE C. HAZA AND TAMAY M. ÖZGÖKMEN

*Rosenstiel School of Marine and Atmospheric Science, University of Miami, Miami, Florida*

ANNALISA GRIFFA

*Istituto di Scienze Marine, Consiglio Nazionale delle Ricerche, La Spezia, Italy*

ANDREW C. POJE

*City University of New York, New York, New York*

M.-PASCALE LELONG

*NorthWest Research Associates, Seattle, Washington*

(Manuscript received 24 May 2014, in final form 23 September 2014)

ABSTRACT

To develop methodologies to maximize the information content of Lagrangian data subject to position errors, synthetic trajectories produced by both a large-eddy simulation (LES) of an idealized submesoscale flow field and a high-resolution Hybrid Coordinate Ocean Model simulation of the North Atlantic circulation are analyzed. Scale-dependent Lagrangian measures of two-particle dispersion, mainly the finite-scale Lyapunov exponent [FSLE; $\lambda(\delta)$], are used as metrics to determine the effects of position uncertainty on the observed dispersion regimes. It is found that the cumulative effect of position uncertainty on $\lambda(\delta)$ may extend to scales 20–60 times larger than the position uncertainty. The range of separation scales affected by a given level of position uncertainty depends upon the slope of the true FSLE distribution at the scale of the uncertainty. Low-pass filtering or temporal subsampling of the trajectories reduces the effective noise amplitudes at the smallest spatial scales at the expense of limiting the maximum computable value of $\lambda$. An adaptive time-filtering approach is proposed as a means of extracting the true FSLE signal from data with uncertain position measurements. Application of this filtering process to the drifters with the Argos positioning system released during the LatMix: Studies of Submesoscale Stirring and Mixing (2011) indicates that the measurement noise dominates the dispersion regime in $\lambda$ for separation scales $\delta < 3$ km. An expression is provided to estimate position errors that can be afforded depending on the expected maximum $\lambda$ in the submesoscale regime.

## 1. Introduction

Understanding the dispersive properties of velocity fluctuations at the ocean's submesoscales is essential for accurately predicting the initial evolution of spatially confined pollutant sources such as oil spills. Because of the small spatial and temporal scales characterizing submesoscale motions (100 m to 10 km, few hours), quantification of dispersion from Lagrangian observations is likely to be sensitive to both position measurement errors and position sampling frequency. The objective of this study is to investigate how observational uncertainty affects scale-dependent relative dispersion in the submesoscale range and how to improve the separation of the signal from inherent measurement errors.

Many coastal and oceanic transport problems—such as the dispersal of fish larvae; the spreading of solid materials, pollutants, and oil spills—require answers to basic questions involving either where the substance

*Corresponding author address:* Angelique C. Haza, Rosenstiel School of Marine and Atmospheric Science, University of Miami, 4600 Rickenbacker Causeway, Miami, FL 33149.
E-mail: ahaza@rsmas.miami.edu

DOI: 10.1175/JTECH-D-14-00107.1

comes from, or where it gets transported, or how fast a tracer patch is expanding. Such studies are most naturally carried out within a Lagrangian framework, involving the solution of

$$\frac{d\mathbf{r}}{dt} = \mathbf{v}(t) = \mathbf{u}(\mathbf{x}, t), \tag{1}$$

where $\mathbf{r}$ is the position vector, $\mathbf{v}(t)$ is the temporal evolution of the Lagrangian velocity vector of a particle along its trajectory, and $\mathbf{u}(\mathbf{x}, t)$ is the corresponding Eulerian velocity field. The dispersive characteristics of a flow field usually require a statistical analysis with a high number of particle trajectories. More specifically, relative dispersion, defined as

$$D^2(t) = \langle (\mathbf{r}_2(t) - \mathbf{r}_1(t))^2 \rangle, \tag{2}$$

is used to quantify the velocity differences between locations, including the net effect of turbulent fluctuations in the underlying flow field and horizontal shear on the separation distance between two particles (denoted by the subscripts). The angle brackets, $\langle\rangle$, in (2) indicate averaging over the available number of particle pairs.

Another metric also based on two-particle statistics is the scale-dependent finite-scale Lyapunov exponent (FSLE; Artale et al. 1997; Aurell et al. 1997), defined as

$$\lambda(\delta) = \frac{\log(\alpha)}{\langle \tau \rangle}, \tag{3}$$

where $\langle \tau \rangle$ is the averaged time taken by all particle pairs to separate from distance $\delta$ to distance $\alpha\delta$. The "doubling" scale $\alpha$ is typically in the range of $1 < \alpha < 2$ (Haza et al. 2008). Unlike the relative dispersion, which averages pair separation distances at a given time, the FSLE metric computes averages of separation times at a given separation distance and has the advantage of isolating differences in dispersion rates due to velocity fluctuations at given spatial scales.

There are various considerations that must be addressed in the computation and interpretation of both $D^2(t)$ and $\lambda(\delta)$. These involve the number of drifters (Lacorata et al. 2001; Özgökmen et al. 2011), initial separation scales and sampling strategies (Özgökmen and Fischer 2012), the use of chance versus original pairs, and sensitivities to the details of the averaging procedure in the FSLE computation (Haza et al. 2008). While random errors in positions of drifters have been highlighted as a potential important error source for velocity gradients on the basis of kinematic flow fields (Kirwan and Chang 1979), as well as from experience in field experiments (Ohlmann et al. 2005), the impact of position and/or velocity errors on two-point dispersion estimates, especially at submesoscale separations, has not been analyzed in much detail.

Drifter position errors require a detailed study because they may adversely impact observations of scale-dependent Lagrangian dispersion metrics providing direct insight into the multiscale interactions in the ocean (Özgökmen et al. 2012). Of particular interest is understanding the nature, location, and dispersive properties of submesoscale fluctuations. The submesoscales are broadly defined as flows immediately below those of the mesoscale, namely, spatial scales from 100 m to 10 km and evolution time scales of hours to days (Thomas et al. 2008). Such flows are typically concentrated within the upper-ocean mixed layer, in the form of frontal instabilities (Boccaletti et al. 2007; Fox-Kemper et al. 2008) or filaments arising from frontogenesis (Capet et al. 2008; Badin et al. 2011; Zhong et al. 2012; Mensa et al. 2013). Dynamically, the controlling effects of geostrophy and strong stratification are no longer entirely dominant at the submesoscales and as such, these spatial and temporal scales are the resolution limit of current operational ocean models.

In the Eulerian frame, active submesoscale motions provide a means for downscale energy cascade from 2D, quasigeostrophically balanced mesoscale eddies to fully 3D motions extending to viscous dissipative scales. As such, they potentially play a significant role in the ocean's energy budget (Müller et al. 2005; McWilliams 2008). In the Lagrangian frame, submesoscale flows may significantly impact the vertical biogechemical transport (Mahadevan and Tandon 2006; Klein and Lapeyre 2009) and may enhance lateral dispersion in the near-surface ocean (Shcherbina et al. 2013).

A main question is the nature of the interaction between, and relative importance of, mesoscale and submesoscale fluctuations on ocean dispersion. Our main interest is differentiating between two hypotheses (Özgökmen et al. 2012): Hypothesis I is that the submesoscale field consists of weak perturbations superimposed on the mesoscale field. Submesoscale eddies are short lasting and transported by the underlying, long-lasting mesoscale eddies, thereby having no major influence on the transport of tracers (e.g., pollutants, oil spills). This *nonlocal* regime (Bennett 1984) is equivalent to a steep kinetic energy wavenumber spectrum, $\mathrm{KE} \sim k^{-\beta}$, with $\beta \geq 3$, so that for particle pair separation distance smaller than the mesoscale deformation radius, $\delta < R_d$, the dispersion rate is scale independent, $\lambda(\delta) \sim \lambda_0$, at submesoscale separations. The constant time scale is controlled by the stretching and folding of mesoscale eddies at significantly larger scale. Hypothesis II is defined as when submesoscale processes are energetically important enough to enhance spectral slope ($\beta < 3$; e.g.,

Capet et al. 2008), and they exert control on relative dispersion at their own scale (*local* regime), leading to a scale-dependent relative dispersion behavior. The practical implication of hypothesis I is that while the current generation of ocean models' assimilating, and accurately modeling, mesoscale features can adequately address transport problems occurring over the submesoscales. On the other hand, hypothesis II implies that large surface dispersion errors are to be expected in models' resolving processes only at the scale $R_d$. Therefore, hypothesis II, where and when applicable, indicates that improvements would be needed in both model resolution and observational capabilities to address submesoscale transport problems.

The scaling laws for relative dispersion have been well-established (Batchelor 1952; Babiano et al. 1990; LaCasce 2008) and how they relate to the underlying (Eulerian) processes have been studied (Bennett 1984; Poje et al. 2010). The scaling behavior is typically classified as the Richardson (Richardson 1926), $D^2 \sim t^3$; ballistic, $D^2(t) \sim t^2$; and diffusive, $D^2(t) \sim t$, regimes. For smooth velocity fields where the local slope of the energy spectrum of the underlying Eulerian velocity field, $E(k) \sim k^{-\beta}$, is steep, $\beta > 3$, an exponential regime is attained, $D \sim e^{\lambda t}$, where $\lambda$ is the Lyapunov exponent, as in Eq. (3). The relationship between other regimes of the FSLE and $D^2$ is established as well (Boffetta et al. 2000). The Richardson regime implies $\lambda(\delta) \sim \delta^{-2/3}$, ballistic motion implies $\lambda(\delta) \sim \delta^{-1}$, and the diffusive regime is given by $\lambda(\delta) \sim \delta^{-2}$.

Scale-dependent Lagrangian measures have been used to explore the net dispersive effect of highly turbulent motions in a number of ocean models (Haza et al. 2008; Poje et al. 2010). In particular, these measures have been put forward as one of the most suitable methods to detect rapidly evolving submesoscale flows (Özgökmen et al. 2011; Özgökmen and Fischer 2012; Özgökmen et al. 2012). Oceanic experiments with an increasing number of drifter pairs over the submesoscale regime have been conducted in the Gulf of Mexico (Ohlmann et al. 2005; LaCasce and Ohlmann 2003), the Gulf Stream region (Lumpkin and Elipot 2010), Nordic seas (Koszalka et al. 2009), southern Atlantic (Berti et al. 2011), and the Mediterranean Sea (Schroeder et al. 2011, 2012). These experiments have revealed that it is a major challenge to differentiate between hypothesis I and hypothesis II, mainly because of the number of drifters needed in closely spaced clusters. Mixed results have been reported between nonlocal and local dispersion regimes. The practical implications of improving our understanding of multiscale interactions in the ocean have fueled the largest synoptic upper-ocean drifter deployment to date, the Grand Lagrangian Deployment (GLAD) in the Gulf of Mexico, in which approximately 300 surface drifters initially sampling separation scales between 100 m to 10 km were deployed over 10 days in the summer of 2012 (Olascoaga et al. 2013; Carrier et al. 2014; Poje et al. 2014).

As large-scale Lagrangian observations focus on rapidly evolving processes at smaller spatial scales, the effects of both inherent uncertainty in drifter position measurements and operational limitations on sampling frequency become increasingly important. The accuracy of position fixes by the Argos system used for most Surface Velocity Program (SVP) drifters (1250 simultaneously in the World Ocean) is estimated to be between 500 and 1000 m (Lumpkin and Pazos 2007). Since these errors are close to the dynamical scales of interest for submesoscale dispersion, a detailed study of their impact is warranted. Higher position accuracies, 5–10 m, can be attained with GPS tracking (Ohlmann et al. 2005) and are becoming widely used for Lagrangian observations beyond the surfzone. Near the coast, it is possible to reduce position errors down to 0.1 m by using the differential GPS, which relies on land-based reference stations to estimate the difference between their fixed positions and the GPS measurements. Recent modeling-based (Haza et al. 2012) and analytical (Piterbarg 2012) studies have increased awareness of the significant effect of stochasticity produced by position uncertainty on relative dispersion estimates. Position uncertainty estimates and data transmission costs typically set the maximum frequency at which positions are sampled. LaCasce (2008) found that $\lambda(\delta)$ estimates from the Surface Current and Lagrangian Drift Program (SCULP) drifter dataset in the Gulf of Mexico were strongly affected by the sampling frequency, with a tendency toward higher estimates at submesoscales when the trajectories were interpolated from daily to hourly values.

Investigating these observational considerations can be done only if we have a prior knowledge of the real signal. For this reason, the most convenient approach is to rely on numerical models as proxy for the surface ocean velocity fields while being aware of the fact that models do not reproduce all the processes occurring in the real ocean. Synthetic trajectories obtained from coastal and ocean models are assumed to be error free, and they are corrupted by using noise to mimic the error in measurements.

The specific questions that we aim to address are as follows:

1) How does the position error affect relative dispersion metrics over the submesoscales?
2) Is it possible to distinguish the noise from the actual submesoscale signal in relative dispersion, so that much of the original dispersion signal is recovered?

3) Since the removal of noise is likely to involve some type of filtering, what is the impact of trajectory filtering on the scale-dependent FSLE?

In this study, we use synthetic trajectories from two models to study these issues. The first set of synthetic trajectories are generated using flow fields from a 1/48° horizontal-resolution Hybrid Coordinate Ocean Model (HYCOM; Chassignet et al. 2006) configured in the North Atlantic (Fig. 1). The model is subject to realistic forcing and boundary conditions in the North Atlantic, focusing on the Gulf Stream extension and recirculation area. We have studied this flow field in order to develop Lagrangian parameterizations of submesoscale dispersion (Haza et al. 2012) and to investigate the seasonality of submesoscales (Mensa et al. 2013). The second set of trajectories is obtained from a flow field generated by large-eddy simulations (LES) of two interacting baroclinic instabilities, namely, submesoscale mixed layer eddies modulated by deeper mesoscale disturbances. The disparate scales of coherent structures arising from these two instabilities are captured in the corresponding $\lambda(\delta)$ (Özgökmen et al. 2012).

The rationale behind the choice of the two models is centered on the dynamics resolved by these simulations with respect to the position error, which can be as high as 1 km. Because of the coarse resolution and parameterized mixed layer dynamics, the HYCOM simulation resolves only part of the submesoscale spectrum, namely, scales larger than 1/24°. As such, separating position noise on the order of 1 km is relatively straightforward. With high-order numerics and mesh spacings going down 17 m in the horizontal, the multiscale LES explicitly captures submesoscale eddies on the scales of 200 m (Özgökmen et al. 2012). Therefore, it is a harder problem to separate signal from noise in this case.

In addition to introducing random position uncertainty in the model-generated synthetic trajectories, we also consider the use of a random walk model. This is because in the oceanographic situation, the corrupted positions constitute the original data. In this case, one cannot use a simple position uncertainty model, since the observations are already uncertain. Instead, we use the random walk model to ask when (at what separation scale) the observed trajectories produce FSLE curves that look like random walk curves. Therefore, in the first part of the paper, we show that random walk and position uncertainty (when the "true" positions are known) models have similar FSLE signatures. In the subsequent part of the paper, we use the random walk model to assess FSLE curves in the situation where the true positions are not known.

The insight developed from these models is then applied to drifter trajectories from a recent Lateral Mixing (LatMix) experiment conducted south of the Gulf Stream in the summer of 2011 in order to distinguish between noise and submesoscale dispersion signal from these trajectories.

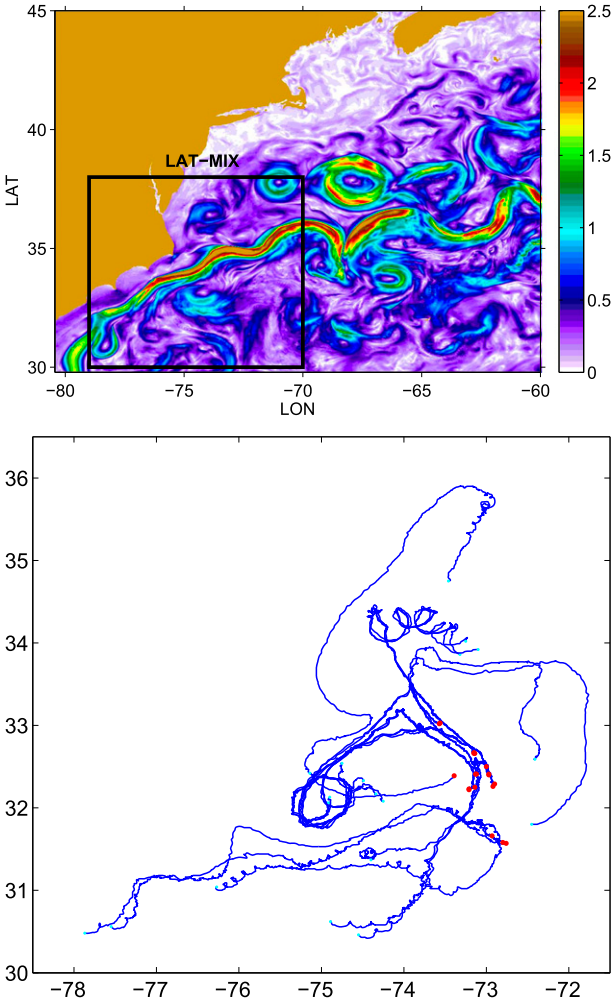


FIG. 1. (top) Snapshot of surface speed over the domain of the HYCOM study. Superimposed is the area covered by the LatMix drifters over the duration of the relative dispersion analysis. (bottom) Three-week LatMix SVP drifter trajectories in June 2011. The drifters were launched at the locations marked by the red points.

The paper is organized as follows: The models and datasets are described in section 2; the methodologies for adding uncertainty to datasets are discussed on section 3. The results are provided in section 4. Finally, a summary and discussions follow in section 5.

## 2. Trajectory datasets

### a. *Submesoscale-permitting ocean general circulation model*

HYCOM 1/48° simulation is centered on the Gulf Stream and nested within a larger-scale 1/12° North Atlantic simulation (Fig. 1). The simulation is performed subject to

atmospheric forcing based on monthly values from the 40-yr European Centre for Medium-Range Weather Forecasts (ECMWF) Re-Analysis, superimposed with 6-hourly anomalies from perpetual-year wind stress and wind speed data from the Navy Operational Global Atmospheric Prediction System (NOGAPS). Details on the model configuration and results can be found in Haza et al. (2012) and Mensa et al. (2013). The horizontal grid spacing of approximately 2 km permits submesoscale features as small as 4 km to be represented.

A total of 5067 surface particles are launched over the whole domain in a triplet configuration composed of pairs separated by a distance of 100 m. These original pairs are used for the computation of the relative dispersion metrics, that is, $D^2(t)$ and $\lambda$ ($\delta$). These synthetic particles are advected offline using a 2-h time step for a total duration of 3 months. The scale-dependent FSLE computed from these trajectories is shown in Fig. 2 (top panel). The FSLE curve shows a plateau for $\delta < 5$ km. This is expected given that over the subgrid-scale range, the particles experience advection by smooth velocity fields. For $\delta$ in the resolved submesoscale range, 5 km $< \delta <$ 10 km, $\lambda$ increases with decreasing $\delta$ reaching $\lambda_{\max} = 0.7\,\text{day}^{-1}$. It was shown in Poje et al. (2010) using the Okubo–Weiss criterion that the value of the $\lambda_{\max}$ is controlled by the hyperbolic partition of the flow field (in the absence of horizontal convergence). A Richardson regime is obtained by the stirring caused by eddies, fronts, and filaments in the mesoscale regime $\lambda \sim \delta^{-2/3}$ for $\delta >$ 10 km. Sensitivity tests have been performed considering a subregion corresponding to the LatMix region in Fig. 1, and the results appear robust.

### b. *LES of multiscale baroclinic instability*

This computational study, involving no particle position or velocity uncertainty, was described in Özgökmen et al. (2012); as such we provide a short description here. The flow field is intended to simulate the interaction of a weak and shallow (20 m deep) mixed layer front with a deep baroclinic instability as an idealized choice for one of the ubiquitous multiscale interactions in the ocean. LES with a high-order (13th order in space) spectral element model is conducted. No external (wind or buoyancy) forcing is applied, and the solution corresponds to adjustment starting from an initial state. The particles are released at different levels in the model in triplets that are 20 m apart from one another during a time period when the turbulent features arising from the interaction of both instabilities are most pronounced. A total of 2601 triplets are released at three levels and advected in 3D online (with model time step and using a high-order spatial discretization). Here, we analyze only the surface trajectories from 2601 particles.

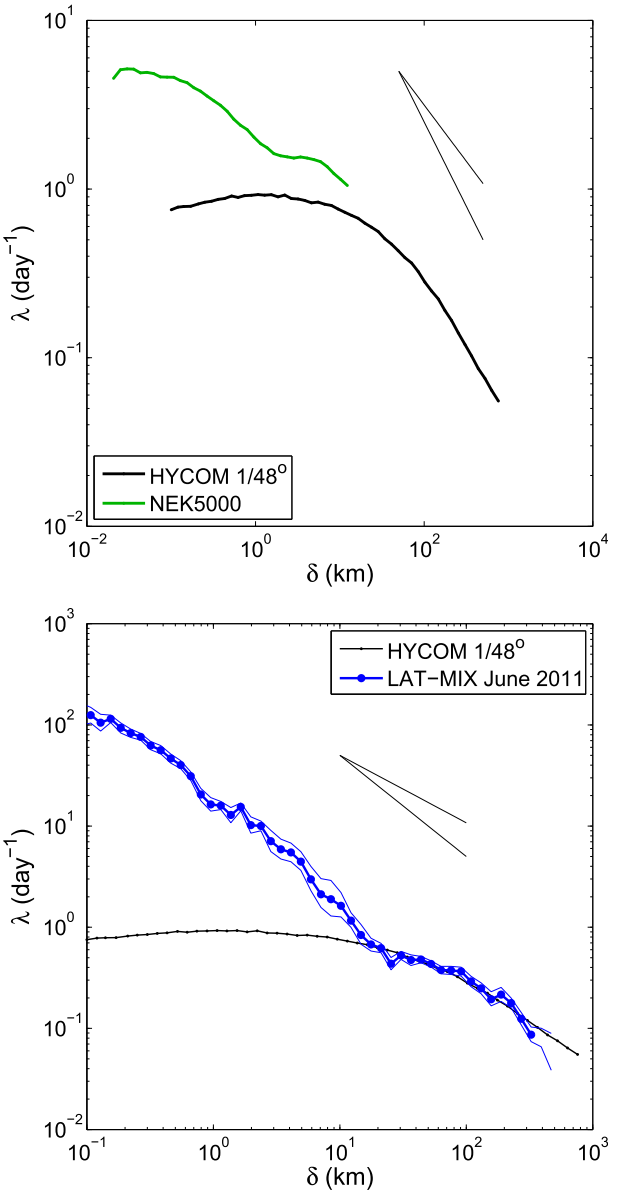


FIG. 2. (top) FSLE $\lambda(\delta)$ from the surface velocity fields of HYCOM (black) and the LES NEK5000 simulation (green). The lines in the background indicate slopes of $-2/3$ and $-1$, corresponding to the Richardson and ballistic regimes, respectively. (bottom) Term $\lambda(\delta)$ from the LatMix SVP drifters (blue) superimposed on that from HYCOM (black). The curves are calculated for pair numbers exceeding 20. The dash lines mark the 95% confidence interval.

Since the model has a rigid lid, these particles stay at the surface and move in 2D only.

In this study, the nondimensional results of Özgökmen et al. (2012) are scaled to match the values of the HYCOM simulations. We scale the velocity scale using the Froude number $\text{Fr} = U(NH) = 0.1$. In particular, we use a buoyancy frequency of $N = 4 \times 10^{-3}\,\text{s}^{-1}$ and maintain the domain scaling of $H = 500$ m, resulting in

a speed scale of $U = 0.2\,\mathrm{m\,s^{-1}}$. The corresponding FSLE curve is shown in Fig. 2 (top-right panel). The maximum FSLE level is $\lambda_{\max} = 5\,\mathrm{day^{-1}}$ at separation scales of tens of meters. A clear Richardson regime is obtained for $100\,\mathrm{m} < \delta < 2\,\mathrm{km}$ due to stirring by submesoscale eddies. The transition to the mesoscale regime, dominated by deeper and larger eddies, occurs for $\delta \geq 7\,\mathrm{km}$. With respect to the HYCOM simulation, the dispersion curve from LES is characterized by stirring from two disparate scales of eddies.

### c. *LatMix drifters*

The LatMix drifter data comprises 3-week trajectories of 20 near-surface SVP drifters released in pairs southeast of the Gulf Stream in June 2011 (Fig. 1, bottom panel). The primary objective of this experiment was to probe the existence and to explore the dynamics of submesoscale features in the summer period. The SVP drifter characteristics are described in Lumpkin and Pazos (2007), and the positioning system carries an uncertainty in range of 500 m to 1 km. The position measurements have an irregular sampling frequency with a median of 1.7 h and a standard deviation of 48 min. The data are interpolated to a regular 15-min interval.

The scale-dependent FSLE from LatMix data is shown in Fig. 2c in comparison to that from HYCOM. We had to rely on chance pairs to compute statistically relevant estimates, as the number of original pairs within a relative distance of 1 km does not exceed 9 in the LatMix data. For scales $\delta > 10\,\mathrm{km}$, the regime is the same as the numerical model, such as the transition from the value $\lambda \sim 0.5\,\mathrm{day^{-1}}$ to the large-scale local regime for $20\,\mathrm{km} < \delta < 100\,\mathrm{km}$, and a Richardson regime at $\delta > 100\,\mathrm{km}$. For $\delta \leq 10\,\mathrm{km}$, the dispersion regime is clearly scale dependent (local), attaining very high values of $O(10\,\mathrm{day^{-1}})$ for $\delta = 1\,\mathrm{km}$ and $O(100\,\mathrm{day^{-1}})$ for $\delta = 100\,\mathrm{m}$. We find a power-law regime of $\lambda \sim \delta^{-1}$ at those scales. The values are significantly higher than those tabulated from previous observational and modeling studies (e.g., Table 1 in Özgökmen et al. (2012)), thereby implying the possibility of a spurious regime created by position uncertainty errors.

## 3. Uncertainty models for trajectories

### a. *Addition of position uncertainty*

In the following, the assumption is made that the model trajectories are the real in situ drifter trajectories: after each integration time step, the new position of a particle advected by the model velocity field is considered the true position. We indicate as $\mathbf{x}^i_{\mathrm{true}}$ the true position at discrete time $i$ of a particle trajectory moving in a flow with velocity $\mathbf{u}$. To simplify the problem, let us assume a simple forward numerical scheme. The position can be written as

$$\mathbf{x}^i_{\mathrm{true}} = \mathbf{x}^{i-1}_{\mathrm{true}} + \Delta t\, \mathbf{u}^{i-1}(\mathbf{x}^{i-1}_{\mathrm{true}}), \tag{4}$$

where $\Delta t$ is the integration time step, and the particle position at time $i$ is function of the model velocity at its previous position corresponding to the time index $i - 1$. In the following applications, the velocity $\mathbf{u}$ is provided by HYCOM and LES.

We assume that the position $\mathbf{x}^i_{\mathrm{true}}$ is measured at each sampling time $i$ with an uncertainty given by random noise, and we indicate the uncertain "corrupted" position as $\mathbf{x}^i_{\mathrm{Cpt}}$, defined as

$$\mathbf{x}^i_{\mathrm{Cpt}} = \mathbf{x}^i_{\mathrm{true}} + L_K\, \mathbf{dW}^i, \tag{5}$$

where $\mathbf{dW}$ is a Gaussian random number drawn from a distribution with zero mean and a standard deviation of 1. Term $L_K$ is the prescribed level of position uncertainty given by the standard deviation of the position measurement error. In the case of the large-scale HYCOM simulation, values for $L_K$ were chosen to match the range of uncertainty typically cited for SVP drifters (Lumpkin and Pazos 2007). In the smaller-scale LES mixed layer simulation, $L_K$ is in the 1–5-m range, which falls in between the expected values of GPS and differential GPS tracking.

In addition to simply adding noise to the particle positions, we also introduce a random walk (rw) model, used for comparison and reference. The reason for considering the random walk is that it provides a model to which one can compare real trajectories. Random walk gives a model with $\lambda(\delta) \sim \delta^{-1}$ for some range of $\delta$ determined by both the uncertainty and the actual velocity. This is essentially the same behavior as one gets when one actually has the true positions and then corrupts this true position with a given level $L_K$ of uncertainty. Although it is different from position uncertainty, we will show in the next sections that it has an identical impact on the FSLE at the scales smaller than $L_K$, despite the fact that it generates relative dispersion cumulating in time. Because of this fundamental difference, the random walk alone or combined with the model velocities is a crucial tool in the following analysis, in particular for the implementation of an adaptive time sampling procedure to reduce uncertainties.

The random walk trajectory in one direction and at time $i$ can be written as

$$x^i_{\mathrm{rw}} = x^{i-1}_{\mathrm{rw}} + \frac{L_K}{\sqrt{2}} dW_x, \tag{6}$$

and it represents the motion of a particle in a random flow, subject to a random displacement at every $\Delta t$. The standard deviation of the displacement $L_K$ is linked in this case to the standard deviation of the turbulent velocity $\sigma_{\rm rw}$, by $L_K \approx \sigma_{\rm rw}\,\Delta t$.

When the random walk is added to the flow velocity $\mathbf{u}$, a ''random walk corrupted'' trajectory $x_{\rm Crw}$ is obtained,

$$x^i_{\rm Crw} = x^{i-1}_{\rm Crw} + \Delta t\, u^{i-1}(x^{i-1}_{\rm Crw}) + \frac{L_K}{\sqrt{2}} dW_x, \qquad (7)$$

where the particle's new position at time index $i$ depends on its previous location, which is function of the model velocity and the random displacement at time index $i-1$.

The $x_{\rm Crw}$ trajectories are inherently different from the $x_{\rm Cpt}$ trajectories. The random walk modifies the integration of the trajectories by adding a random displacement at each time step that cumulates in time, while in $x_{\rm Cpt}$ the noise only affects the measure of the trajectory at each given time. This difference is illustrated in Fig. 3, and it is highlighted in the following expressions. If we assume that the trajectories start from a given position $x^0$, we obtain for the true trajectory $x$ the following:

$$x^i_{\rm true} = x^0 + \Delta t \sum_{k=0}^{i-1} u^k(x^k_{\rm true}), \qquad (8)$$

while for the trajectory measured with uncertainty, one gets

$$x^i_{\rm Cpt} = x^0 + \Delta t \sum_{k=0}^{i-1} u^k(x^k_{\rm true}) + \frac{L_K}{\sqrt{2}} dW^i_x, \qquad (9)$$

and for the random walk affected trajectory, one gets

$$x^i_{\rm Cwr} = x^0 + \Delta t \sum_{k=0}^{i-1} u^k(x^k_{\rm Crw}) + \frac{L_K}{\sqrt{2}} \sum_{k=0}^{i-1} dW^k_x. \qquad (10)$$

### b. *Temporal sampling and filtering*

In the oceanographic community, trajectory observations are often low-pass filtered in time, typically to remove the effects of inertial oscillations or to prepare the data for assimilation (Carrier et al. 2014). The common assumption is that this procedure does not have a serious impact on the postanalysis, even though subinertial motions are clearly filtered out. As interest (and modeling capabilities) move increasingly toward characterizing processes at smaller space and time scales, the effects of temporal filtering are less easily ignored (LaCasce 2008). While more sophisticated filtering processes exist (Hansen and Poulain 1996), the low-pass filter in this study consists of a simple moving nonweighted average along the trajectory with time windows chosen to match the spatial scales of interest (1/3–1.5 days for HYCOM, 1–3 h for LES).

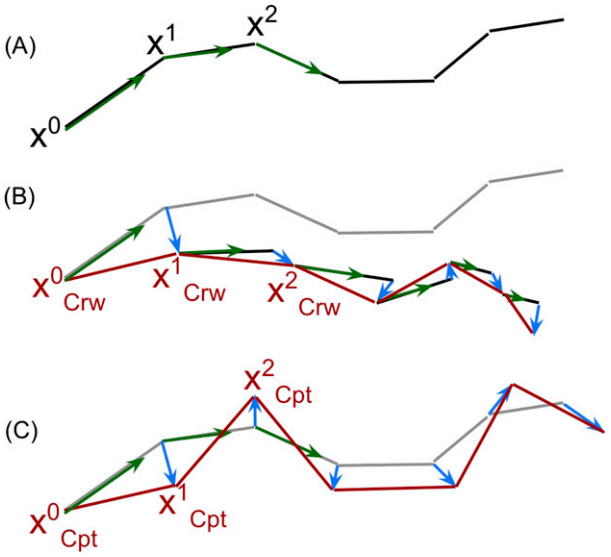


FIG. 3. Schematic diagram illustrating the differences between random walk and position uncertainty. (a) A particle is advected from position $\mathbf{X}^0$ by the model velocity (green vector) during an integral time step $\Delta t$. (b) The corruption by a random walk at every time step is equivalent to a displacement $\mathbf{dW}$ (blue vector) and leads to different positions $\mathbf{X}^i_{\rm Crw}$ diverging from the model trajectory (gray). (c) The corruption by position uncertainty is equivalent to adding a random displacement directly to the model trajectory at each measurement with a sampling time $\Delta t$. The ''observed'' trajectory is then $\mathbf{X}^i_{\rm Cpt}$, and is always within one random displacement of the real position.

For each observation $\mathbf{x}$ at time index $i$, the time length $N+1$ of the temporal moving average is

$$\tilde{\mathbf{x}}^i = \frac{1}{N+1} \sum_{i-N/2}^{i+N/2} \mathbf{x}^k. \qquad (11)$$

For uncertain positions $\mathbf{x}_{\rm Cpt}$ [Eq. (5)], the averaging is equivalent to low-pass filtering true trajectory data and the noise contribution separately. Considering only the zonal position,

$$\widetilde{x^i_{\rm Cpt}} = \widetilde{x^i_{\rm true}} + \frac{L_K}{\sqrt{2}} \widetilde{dW^i_x}.$$

Since the position uncertainty is assumed Gaussian, $\widetilde{\mathbf{x}^i_{\rm Cpt}} \rightarrow \widetilde{\mathbf{x}^i_{\rm true}} \pm L_k/\sqrt{N}$ for moderate values of $N$. In this case, low-pass filtering the uncertain observations is equivalent to adding noise to the filtered original signal with increments defined by $\widetilde{\mathbf{dW}}$, a new Gaussian increment with zero mean and a standard deviation, $\sigma^2 = L_k^2/N$, that decreases with increasing filter length.

Subsampling in time is a very simple form of a low-pass filter, acting mostly on noise. As such it will be investigated here and compared with the low-pass filtering results. Also, subsampling will be explored as a way to evaluate the impact of the temporal resolution of drifter positions on submesoscale relative dispersion. It is known that the FSLE can be prone to aliasing issues based on the temporal resolution of drifter positions. This leads to a requirement on the ratio $\alpha$, which has to be as small as possible to capture all scales of motion, yet higher than a critical value below which $\lambda$ can exhibit a spurious exponential regime (Lacorata et al. 2001). According to Haza et al. (2008), the value of $\alpha$ needs to be larger than $\alpha_{\min} = 1 + \Delta t \Delta v/\delta_0$, where $\Delta t$ is the temporal resolution and $\Delta v$ is the velocity difference of particle pairs at the smallest separation scale considered, $\delta_0$.

Our assumption is that, while not all scales of motions may be resolved by a given position sampling frequency, the cumulative impact of all these motions on drifter pair separations over time is felt at the next sampling time. Note that this is a distinct problem from drifter position errors, since it emerges even if there are no position errors. Yet it is an important consideration for practical applications, since the ocean is full of processes acting at different scales of motion and there are limitations to gathering data; in particular, the satellite data transmission can be a significant part of the total cost, as it is prohibitively expensive to recover drifters in many open ocean applications. The impact of time subsampling on the estimation of relative dispersion is explored by simply subsampling the raw synthetic trajectories, sampled at a given $\Delta t_0$, at larger time intervals ranging from 6 to 36 h in HYCOM and from 1 to 3 h in the LES.

### c. *On the effect of position uncertainty on dispersion*

We look first at the random walk FSLE, as the final expression is more straightforward. The behavior of $\lambda(\delta)$ for a pure random walk has been explored in Piterbarg (2012) and Haza et al. (2012). The relative velocity of particle pairs $V_{\rm rw}$ of a pure random walk is constant at scales $\delta \le L_K$, independent of the separation scale and proportional to the standard deviation of the imposed velocity fluctuations,

$$\Delta V_{\rm rw} \sim \sigma_u = \frac{L_K}{\Delta t}. \tag{12}$$

If $\tau(\delta, \alpha)$ is the average time of a particle pair ensemble to separate from $\delta$ to $\alpha\delta$, then we also have

$$\Delta V_{\rm rw} = \frac{(\alpha - 1)\delta}{\tau(\delta, \alpha)}. \tag{13}$$

It follows that

$$\lambda(\delta) = \frac{\log(\alpha)}{\tau(\delta, \alpha)} \sim \frac{\log(\alpha)}{(\alpha - 1)\Delta t}\frac{L_K}{\delta}, \tag{14}$$

indicating that the random walk contribution to the separation rate for $\delta \le L_K$ decays both with increasing separation distance, $\lambda(\delta) \sim \delta^{-1}$, and with increasing time sampling period $\Delta t$, $\lambda(\delta) \sim \Delta t^{-1}$. For scales $\delta > L_K$, $\lambda(\delta)$ gradually transitions to a $\delta^{-2}$ power-law characteristic of the diffusive regime. There is, however, no analytical expression corresponding to the normal distribution of $\mathbf{dW}$ (Piterbarg 2012).

In the case of position uncertainty $\mathbf{x}_{\rm Cpt}$, similar assumptions can be made for $\Delta V$ when the separation of particle pairs is negligible in comparison to the noise contribution. Such a situation is insured at separation scales $L$ near $L_K$,

$$\Delta V_{\rm Cpt} = \frac{L}{T} \sim \frac{L_K}{\Delta t}, \tag{15}$$

and the average separation rate scales as $\lambda(\delta) \sim \delta^{-1}$, as in the random walk. The scale-dependent FSLE of both $\mathbf{x}_{\rm Cpt}$ and $\mathbf{x}_{\rm Crw}$ are therefore identical at scales $\delta \le L_K$.

On the other hand, their relative dispersions are dramatically different. The effects of position uncertainties, $\mathbf{x}_{\rm Cpt}$, on the behavior of observed time-dependent relative dispersion are readily estimated. If $\mathbf{X}_1(t) = (x_1, y_1)$ and $\mathbf{X}_2(t) = (x_2, y_2)$ are vector positions of a pair of particles at time $t$, then the relative dispersion $D^2(t)$ defined in Eq. (2) is the time evolution of the averaged relative distance of all particle pairs.

For uncertain positions, $\mathbf{X}_{\rm Cpt} = [x_{\rm true} + (L_K/\sqrt{2})dW_x, y_{\rm true} + (L_K/\sqrt{2})dW_y]$, the relative dispersion becomes

$$\begin{aligned} D^2_{\rm Cpt}(t) &= \langle (x_{2\rm true} - x_{1\rm true})^2 \rangle + L_K^2 \langle dW_x^2 \rangle \\ &\quad + \langle (y_{2\rm true} - y_{1\rm true})^2 \rangle + L_K^2 \langle dW_y^2 \rangle \\ &= D^2_{\rm true}(t) + 2L_K^2, \end{aligned} \tag{16}$$

since $\langle dW_x^2 \rangle = \langle dW_y^2 \rangle = 1$. Therefore, at small times when $D^2_{\rm true}(t) \ll L_K^2$, $D^2_{\rm Cpt}(t) \approx L_K^2$ and at larger times when $D^2_{\rm true}(t) \gg L_K^2$, $D^2_{\rm Cpt}(t) \approx D^2_{\rm true}(t)$.

In the case of random-walk-affected trajectories $\mathbf{X}_{\rm Crw}$ [cf. Eqs. (7) and (10)], the random terms are correlated with the velocity through the positions, and the overall effect of the noise cannot be linearized. In fact,

$$D^2_{\rm Crw}(t) \gg D^2_{\rm true}(t) + D^2_{\rm rw}(t) \tag{17}$$

at large times, where $D^2_{\rm rw}(t) \sim 2Kt$ and $K = L_K^2/2\Delta t$ being the diffusivity of the random walk process.

Relative dispersion averages separation distances at a given time. Unlike that of a particle pair with simple position uncertainty imposed at discrete times, the separation distance of a particle pair undergoing a random walk at a given time is the cumulative sum over all increments of the walk up to that time. In contrast, the finite-scale Lyapunov exponent averages separation times at a given separation distance. The average time to separate at a given distance is directly related to the average velocity difference at a given scale. While the separation distance in a random-walk representation is cumulative, the velocity differences at a given time are not. Therefore, FSLE curves for both models behave similarly.

## 4. Results

### a. *Impact of position uncertainty*

FSLE curves produced by HYCOM trajectories with position uncertainties, $\mathbf{x}_{\mathrm{Cpt}}$, and with random walk, $\mathbf{x}_{\mathrm{Crw}}$, for $L_K = 500$ m and 1000 m are shown in Fig. 4a. These values of position uncertainty produce significant changes in relative separation rates for scales up to $\delta \approx 30$ km, close to the mesoscale radius of deformation. The noise results in an increase of $\lambda$ by a factor of 10 around $\delta = 1$ km and a factor of 100 at $\delta = 100$ m. As expected from Eqs. (12) and (15), both Gaussian position uncertainty and random walk models result in a noise-induced, scale-dependent (local) regime with $\lambda \sim \delta^{-1}$ behavior for $\delta < 2L_K$ and time scales near the prescribed sampling period $\Delta t_0 = 2$ h.

As explained above and indicated by Eqs. (16) and (17), the relative dispersion metric provides a means of directly distinguishing between the effects of position uncertainty and random walk. The evolution of the relative dispersion $D^2(t)$ for the HYCOM data is shown in Fig. 4b. The black line shows the dispersion for the original data, $D_{\mathrm{true}}$, for comparison. The trajectories with uncertainty $\mathbf{x}_{\mathrm{Cpt}}$ show a plateau at small scales of order $L_K$, while they converge to $D_{\mathrm{true}}$ at larger scales, as expected. The trajectories with random walk $\mathbf{x}_{\mathrm{Crw}}$, instead, show the expected cumulative effect of velocity correlations in the random walk model. The random walk process effectively adds relative dispersion incrementally, which contributes to a dramatic enhancement of the relative dispersion after a few days, while position uncertainties never contribute more than $2L_K^2$ to $D^2(t)$. This is an important result, because any physical force acting on a pair of drifters will generate time-cumulative dispersion, and as such the impact of position uncertainty constitutes a lower bound (equal to zero), hence a means to distinguish noise from real signal. The results also imply that drifters have to be designed very carefully to avoid accumulation of position errors, such as those that can result from windage or slip with respect to water parcels, due to inertial effects.

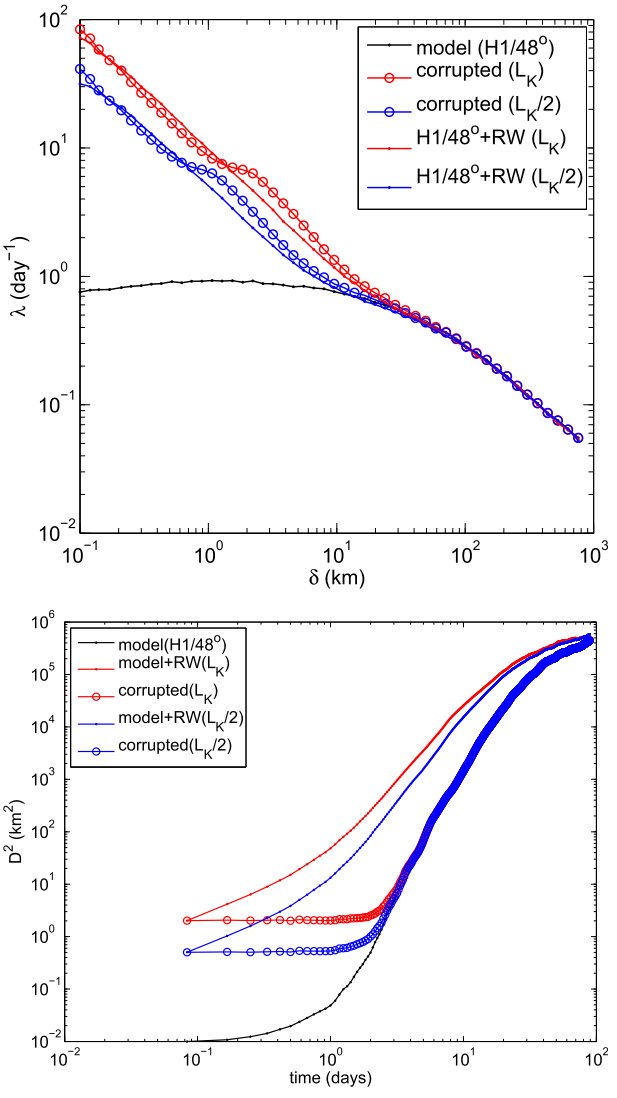


FIG. 4. (top) FSLE $\lambda(\delta)$ from HYCOM (black, denoted $H^1/_{48^\circ}$) corrupted with position uncertainty with amplitudes $L_K = 1000$ m and $L_K/2 = 500$ m every 2 h (lines with red and blue circles, respectively) are superimposed on $\lambda(\delta)$ of HYCOM corrupted with random walk with same $L_K$s and 2-h advection time step. (bottom) As in (top), but for the relative dispersion $D^2(t)$.

In the HYCOM simulation with a well-defined exponential, the nonlocal dispersion regime at scales below 10 km, the FSLE results imply that position errors may affect dispersion metrics at scales considerably larger than the uncertainty scale, and that they can easily be confused with local, scale-dependent dispersion produced by submesoscale processes. Even for the lower uncertainty estimate, $L_K = 500$ m, the observed FSLE curve erroneously indicates local dispersion at all scales,

and the true dispersion rate is only recovered for $\delta >$ 10 km, or at $\delta \sim 20L_k$, coinciding with separation scales where resolved mesoscale structures in the model produce a true local dispersion regime.

The effects of position noise on observed separation rates for the LES mixed layer model are shown in Fig. 5. In contrast to HYCOM, which produces an extended FSLE plateau across the submesoscales, the LES model shows more complex scale dependence including local dispersion for 100 m $< \delta <$ 2 km due to energetic, small-scale mixed layer instabilities; a local plateau (2 km $< \delta <$ 5 km); and a second local dispersion regime for $\delta >$ 5 km produced by the larger, mesoscale motions in the model. In this case, the position uncertainty scales were taken to be $L_K$ = 1 and 5 m with time sampling at 1.5 min. Comparison to those from HYCOM results shown in Fig. 4a shows that there are distinct differences in the observed FSLE curves for the submesoscale flow when the position uncertainty increases from 1 to 5 m. Term $L_K$ = 5 m completely swamps the contribution of the small-scale instabilities, eliminating the small-scale plateau and overpredicting dispersion rates at all scales below ~300 m, nearly 60 times the uncertainty scale. For $L_K$ = 1 m, the local dispersion regime produced by the small scales is accurately captured for $\delta >$ 50 m.

For the FSLE metric, the range of scales adversely effected by position uncertainties of given amplitude depends on the shape of the true FSLE curve and the level of uncertainty. A direct comparison of the results for HYCOM and LES model is shown in Fig. 6, where $\lambda$ is plotted versus $\delta$ normalized by $L_K$. In the HYCOM case, where the level of position uncertainties lies well below separation scales showing local dispersion, there is a clear collapse of the curves $\delta/L_k < 20$. In the LES simulation where there are indications of local dispersion at almost all scales, the collapse is less clear but the effects of position uncertainty extend significantly further to approximately $\delta/L_k \sim 30$.

Given the increasing interest in quantifying dispersion and transport at the submesoscales via Lagrangian-based observations, a method to best extract dispersion metrics from inherently uncertain position measurements, sampled with necessarily limited frequency, is needed. This problem is explored with data subsampling.

### b. *Time subsampling, filtering, and interpolation*

Equation (15) explains both the identical $\lambda$ ($\delta$) signatures at small scales observed in trajectories with position uncertainties and with random walk, as well as the role played by the sampling frequency in setting the amplitude of the noise-induced dispersion error. For fixed measurement error with a standard deviation of $L_K$, the dispersion rate error increases with increased

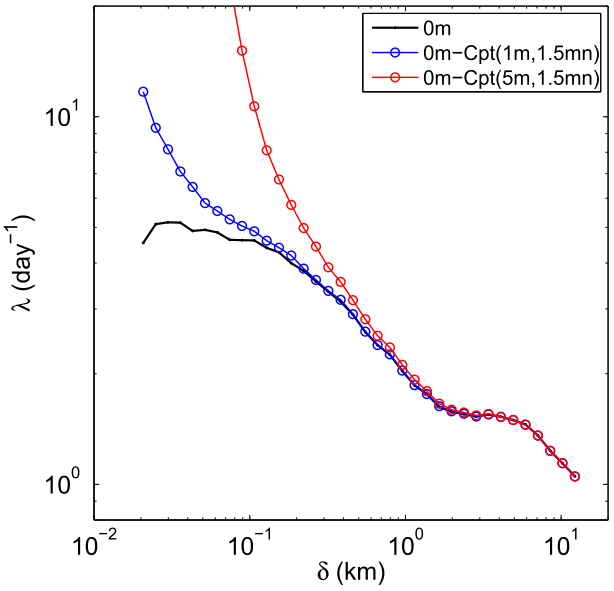


FIG. 5. FSLE $\lambda(\delta)$ from the LES mixed layer simulation (black) computed using position uncertainties with amplitudes $L_K$ = 1 m and $L_K$ = 5 m (lines with red and blue circles, respectively).

sampling frequency (reduced $\Delta t$). Therefore, even relatively small position uncertainties of a few meters instead of kilometers may yield erroneously high FSLE estimates for $\Delta t \ll$ 2 h. This dependence is especially relevant for the high-frequency sampling of GPS-tracked drifters used to observe evolving small-scale, submesoscale ocean features.

Since the range of the noise-dominated portion of $\lambda$ depends in part on the sampling frequency, we first examine the effects of simple subsampling on FSLE observations produced by the original HYCOM trajectories. As illustrated in Fig. 7, coarsening the temporal resolution of trajectories leads to aliasing errors in the computation of the FSLE at the highest separation rates, typically occurring at the smallest separation scales. The degree of aliasing increases as the value of $\alpha$ decreases and/or the true separation rate increases. Aliasing due to inadequate sampling frequency or subcritical values of $\alpha$ necessarily biases the observed values of $\lambda$ ($\delta$) downward. For fixed values of $\Delta t$, the schematic indicates that estimates of $\lambda$ ($\delta$) can be improved by simply linearly interpolating in time the relative distances of each particle pair.

Results are shown in Fig. 8 (left panel) for the HYCOM trajectories $\mathbf{x}_{\text{true}}$. The solid curves show the results for trajectories subsampled at 6-, 12-, and 24-h intervals corresponding to subsampling the original trajectories at 3, 6, and 12 times the original $\Delta t$ = 2 h period. When the actual average separation time of particle pairs approaches the imposed trajectory sampling period, the

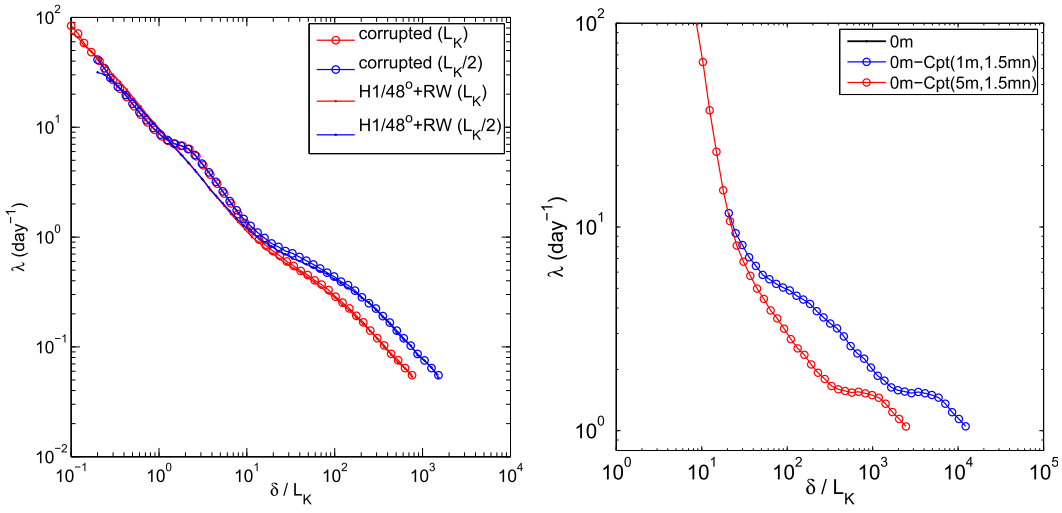


FIG. 6. (right) FSLE $\lambda(\delta)$ from corrupted and random walk trajectories from HYCOM simulation as a function of the separation scale normalized by $L_K$. (left) As in (right), but for the LES mixed layer model.

maximum observable value of the separation rate can be estimated by

$$\lambda_{\max} \approx \frac{\log\alpha}{2\Delta t}. \tag{18}$$

This scaling, shown by the dashed lines on the figure, closely matches the linear decrease in the observed limiting values of $\lambda$ with the subsampling period. Term $\lambda(\delta)$, computed by linearly interpolating pair separations in time, are shown by the curves with symbols. Linear interpolation clearly allows significant improvements in the ability to estimate $\lambda(\delta)$ at scales where position sampling rates approach the average pair separation rate. The effect of sampling frequency on FSLE curves, using linear interpolation, is shown for the mixed layer instability (MLI)–LES data in the right panel of Fig. 8. While estimates from temporally subsampled trajectories, regardless of interpolation, will necessarily provide only lower bounds on the actual separation rates, results for both models indicate that linear interpolation provides an appreciable decrease in the dependence of $\lambda(\delta)$ on the data subsampling interval.

The impact of filtering/subsampling the trajectories differs between HYCOM and the MLI–LES experiment, as it depends also on the spatial scale. The time scales governing the relative dispersion at the submesoscales are controlled by the smallest resolved features setting the rate of pair separation. In HYCOM, the smallest features have a length scale of about 5 km (twice the grid spacing) and time scales of more than a day, that is, slightly above the range of the filtering periods. As the time window is increased from 12 to 36 h, the FSLE plateau is only moderately reduced by subsampling at the scales below 5–10 km, where $\lambda_{\max}$ asymptotes to a threshold of 0.5 day$^{-1}$. In the MLI-LES experiment, the 20–100-m scales are affected the most, while the 100–1000-m scales (from the mixed layer instabilities) are less affected with the increasing scale. It is consistent with small circulation features having shorter time scales than bigger features, hence being more altered by coarser time sampling.

The effects of position uncertainty for the HYCOM trajectories is now investigated with a $L_K = 1000$ m noise. The $\mathbf{x}_{\text{Cpt}}$ trajectories are low-pass filtered by either subsampling (Fig. 9, top panel) with a $\Delta t = 6$, 12, and 24 h, or

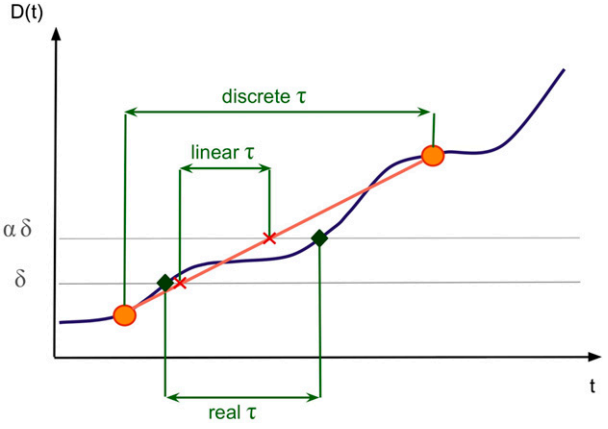


FIG. 7. Schematic illustration of the error in $\tau$ introduced by discrete time sampling of the trajectories (marked by the orange dots) in comparison to the real $\tau$ it takes for particles to separate from $\delta$ to $\alpha\delta$. Improvement of error by linear interpolations between subsampling points (denoted linear $\tau$) is also shown.

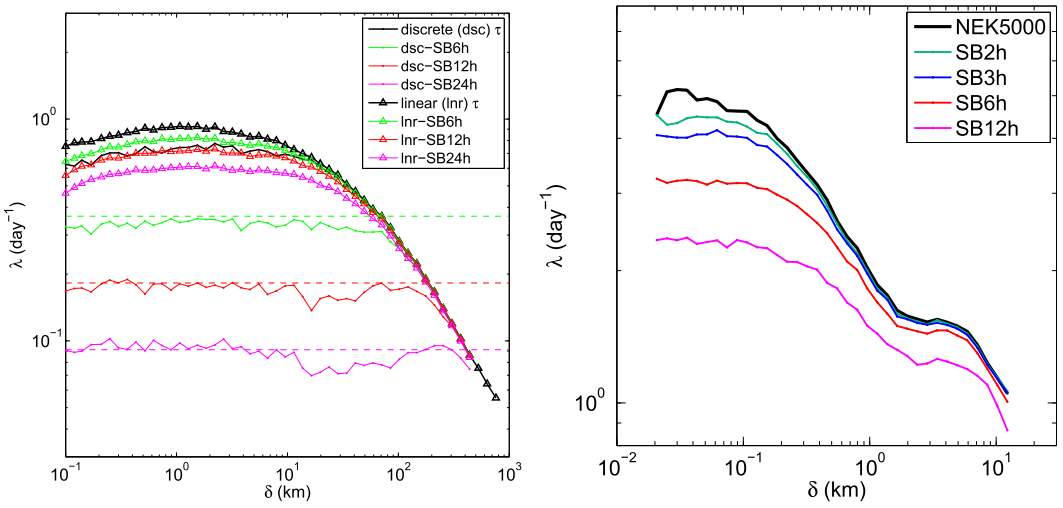


FIG. 8. (left) FSLE $\lambda(\delta)$ computed from HYCOM trajectories subsampled every 6, 12, and 24 h by using either a discrete number of the sampling interval for computation of $\langle\tau\rangle$ (dots) or by linearly interpolating in time the relative distances of each particle pair (triangles). (right) The dashed lines correspond to $\lambda = \log(\alpha)/(2\Delta t)$. Term $\lambda(\delta)$ computed from the LES mixed layer model by linear time interpolation.

by a moving time average (Fig. 9, bottom panel) with a period $T_{\mathrm{LPt}} = 12$, 24, and 36 h. In all experiments, the FSLE curves display substantially lower values, indicating a reduction of the noise contribution. As the filtering period (i.e., $\Delta t$ or $T_{\mathrm{LPt}}$) increases, bigger portions of the original FSLE are recovered, albeit their filtered counterparts. For example, a 12-h subsampling removed the noise contribution at the scales 4 km $\leq \delta \leq$ 40 km, while the 12-h time-average removes it at 5 km $\leq \delta \leq$ 40 km. For a 24-h filtering, the FSLE of the 1-day filtered trajectories is recovered down to $\delta \approx$ 1–2 km. One can see that the rapid variance reduction produced by temporal subsampling (or equivalently, low-pass filtering) has a far more pronounced effect on the noise-induced FSLE errors produced by inherent position uncertainties. This behavior discrepancy is what allows for differentiating the real signal from the corrupted part.

In all cases, the noise-dominated signal still displays a $\delta^{-1}$ regime at the scales $\leq L_K$. For the subsampling, the reason is pretty straightforward: at these scales, the averaged relative velocity $\Delta V_{\mathrm{Cpt}}$ is proportional to the measurement sampling frequency $1/\Delta t$ [cf. Eq. (15)]. Therefore, coarsening the time sampling reduces $\Delta V_{\mathrm{Cpt}}$ independently of $\delta$, resulting also in a $\delta^{-1}$ regime.

For the time-average filter, let us assume that the zonal velocity along a trajectory at time index $i$ is

$$u^i \approx \frac{x^{i+1} - x^i}{\Delta t}. \tag{19}$$

Then for a time average of $T_{\mathrm{LPt}} = (N+1)\Delta t$, the new zonal velocity becomes

$$\tilde{u}^i \approx \frac{\widetilde{x^{i+1}} - \tilde{x}^i}{\Delta t} = \frac{1}{\Delta t}\frac{1}{(N+1)}\left(\sum_{i+1-N/2}^{i+1+N/2} x^j - \sum_{i-N/2}^{i+N/2} x^k\right), \tag{20}$$

leading to

$$\tilde{u}^i \approx \frac{x^{i+1+N/2} - x^{i-N/2}}{(N+1)\Delta t}. \tag{21}$$

Equation (21) indicates that the time average affects the Lagrangian velocities in a way that is very similar to subsampling. Therefore, the zonal velocity of filtered corrupted trajectories is

$$\widetilde{u^i_{Cpt}} \approx \tilde{u}^i + \frac{dW^{i+1+N/2} - dW^{i-N/2}}{(N+1)\Delta t}, \tag{22}$$

resulting in

$$\widetilde{\Delta V_{\mathrm{Cpt}}} \sim \frac{L_K}{(N+1)\Delta t} = \frac{L_K}{T_{\mathrm{LPt}}} \tag{23}$$

for the averaged relative velocity of the position uncertainty with $T_{\mathrm{LPt}} = (N+1)\Delta t$.

In agreement with Eqs. (15) and (23), low-pass filtering the uncertain trajectories and rescaling $\lambda$ by the inverse of either the sampling interval (subsampling) or the inverse of the time window (time averaging) leads to a collapse of the curves at the scales where the position uncertainty dominates the signal. Figure 10 illustrates the collapses of the subsampled (top panel) and time-averaged (bottom panel) experiments. In the latter case, trajectories with a different position uncertainty

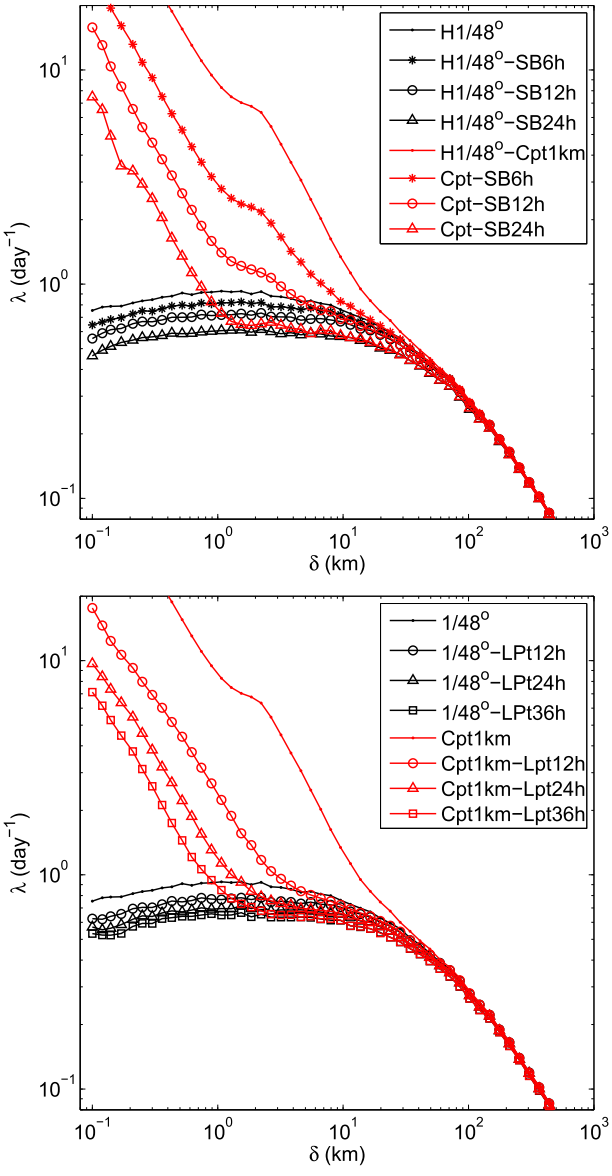


FIG. 9. (top) FSLE $\lambda(\delta)$ from HYCOM trajectories corrupted using $L_K = 1000$ m and subsampled with $\Delta t = 6$, 12, and 24 h. (bottom) As in (top), but showing the effects of low-pass filtering the original trajectories with time windows of 12, 24, and 36 h.

of $L_K = 500$ m and $\Delta t = 2$ h are also included in the figure, and $\delta$ is rescaled by $L_K$ to illustrate the general trend of Eq. (14) corresponding to

$$\lambda^* \sim \frac{\log(\alpha)}{\alpha - 1}\frac{1}{\delta^*} \quad \text{with} \quad \lambda^* = \lambda T_{\mathrm{LPt}} \quad \text{and} \quad \delta^* = \delta / L_K . \tag{24}$$

### c. *Adaptive filter to recover signal*

An adaptive filtering technique can be developed based on two factors: first, the knowledge of the position uncertainty contribution in the FSLE, which can be estimated from an uncorrelated random walk with the same parameters ($L_K$, $\Delta t$); second, and due to the generation of cumulative dispersion by the flow features at all scales, the FSLE of the real trajectories is less affected by low-pass filters than the noise. As a result, filtering drifter trajectories by either subsampling or using a simple time average with increasing time intervals/periods can reduce the noise contribution down to negligible levels with respect to the FSLE of the measured filtered trajectories.

The method is as follows: the measured FSLE of the drifter trajectories is compared to the FSLE of a pure random walk with the given (assumed known) value of $L_K$ and $\Delta t$ equal to the sampling frequency of the Lagrangian observations. Similarities of the position uncertainty and random walk FSLEs are presented in the appendix. The range of scales affected by the noise corresponds to the spatial scales where the noise-induced FSLE signal is equal to or higher than the measured signal. We then proceed to subsample the trajectories with increasing time intervals (or increasing time windows if using low-pass filtering) and to compare the resulting signal to the FSLE of a random walk with the same sampling frequency as the filter. Once the noise-induced FSLE has decreased to levels substantially lower than the FSLE of the filtered trajectories, it is no longer affecting the real signal. The optimal recovered signal is therefore the FSLE of the filtered trajectories with the smallest $\Delta t$ or averaging period $T_{\mathrm{LPt}}$ necessary to distinguish the noise from the FSLE of the filtered trajectories.

Examples of the effectiveness of this approach are presented in Fig. 11 for both the HYCOM and MLI–LES data. For random position errors of $L_k = 1$ km and raw sampling period $\Delta t_0 = 2$ h in the HYCOM experiment, subsampling the trajectories up to $\Delta t = 1$ day results in recovery of the original 1-day subsampled curve for separation scales $\delta > 3$ km. The smaller scales are still corrupted by the position uncertainty, as evidenced by the equally high values of the filtered measured signal and the pure random walk model with $L_k = 1$ km with a 1-day sampling period.

The LES–MLI simulation, shown in the bottom panel of Fig. 11, presents a more challenging problem. Unlike HYCOM with an extended range of constant, scale-independent dispersion rates, the active submesoscale motions in the mixed layer simulation produce scale-dependent dispersion across all observable separation scales. In the mesoscale-dominated OGCM, it is a relatively simple task to filter out the scale-dependent, noise-induced component from the true, scale-independent signal. The LES–MLI flow requires separating the scale-dependent signal produced by

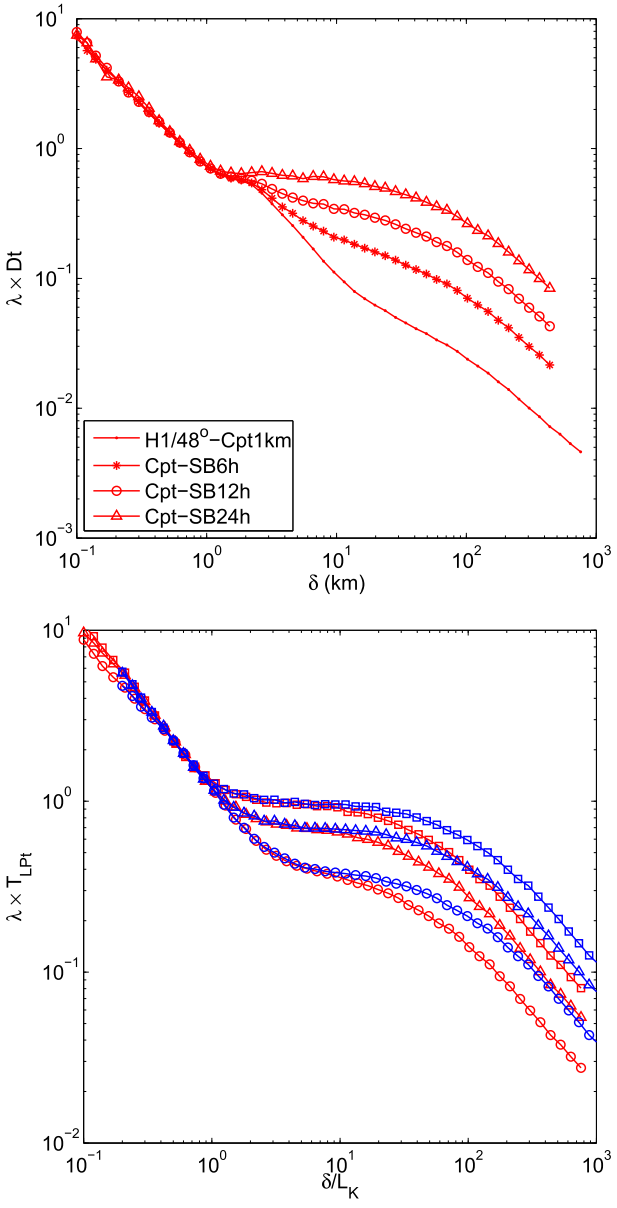


FIG. 10. (top) Term $\lambda(\delta)$ rescaled by the sampling period $\Delta t$ for the subsampled trajectories shown in Fig. 9. (bottom) Results for the low-pass filtered trajectories with $\delta$ rescaled by $L_K$ and $\lambda$ rescaled by the inverse of the time window $T_{\mathrm{LPt}}$. The red curves correspond to position uncertainty $L_K = 1$ km as shown in Fig. 9, while the blue curves indicate results with $L_K = 500$ m.

position uncertainty from the true, scale-dependent signal. For position uncertainties $L_K = 5$ m, the effect of subsampling the original $\Delta t_0 = 90$ s signal to $\Delta t = 30$ min is shown in Fig. 11. While the collapse of the extracted signal to the pure noise signal is slower than that seen in the HYCOM data, similar scaling for the two curves is observed for $\delta \lessapprox 50$ m and the signal from the filtered, uncertain observations accurately predicts the true signal for all $\delta > 200$ m.

### d. *LatMix drifters*

Following the methodology of the previous sections, the LatMix trajectories are subject to low-pass filtering from a time moving average, with windows of 6, 12, and 24 h. The corresponding $\lambda$ and pair numbers are plotted in the top panel of Fig. 12. One can see that the trajectory filtering affected the signal for $\delta < 20$ km, while the larger scales are robust to the low-pass filter. In particular, the 6-h time average reduces $\lambda$ dramatically at the submesoscales, down by a factor of 5 at $\delta = 100$ m. At the junction corresponding to the 7–20-km scale range, a bump in the curve emerges from the 6-h filtering and remains unaffected by the other time averages.

Note that the low-pass filter tends to reduce substantially the number of pairs at the small scales, from more than 200 to around 50 for the 6-h time average. As the filtering strength increases, the pair availability goes down to the critical 10, below which the FSLE curve would be statistically irrelevant. For this reason we chose to plot $\lambda$ for a minimum of 10 pairs. A minimum of 20 pairs would already remove parts of the curves below 1 km for the 12- and 24-h low-passed trajectories. This issue is aggravated by the already limited dataset of only 20 drifters, which is why an experiment tailored for scale-dependent relative dispersion would benefit from at least 100 drifters.

Term $\lambda$ is then rescaled by the inverse of the time window $T_{\mathrm{LPt}}$ to check on the noise impact. The bottom panel of Fig. 12 displays the collapse of all the curves for $100\ \mathrm{m} < \delta < 1000$ m. The FSLE over this scale range is therefore dominated by the noise from position errors. The raw trajectory curve is also added to the figure and the collapse occurs for a $T_{\mathrm{LPt}} = 1$ h. It indicates that the effective time interval dominating $\lambda$ is $\Delta t = 1$ h, even if the averaged sampling interval of the data is 1.7 h. This result is consistent with other tests (not shown), leading to the conclusion that a higher sampling frequency will impose statistically the noise specifics in the computation of the FSLE. For the LatMix experiment, the frequencies higher than the mean (and/or median) have contributed to a stronger noise than predicted by the averaged sampling frequency.

We now proceed to recover the original signal via the adaptive filtering technique. As illustrated in Fig. 13, the random walk FSLE with the drifter uncertainty standard deviation $L_K$ and sampling frequency $\Delta t = T_{\mathrm{LPt}}$ is superimposed on the FSLE of the filtered LatMix trajectories. For the raw data, the portion of the curve significantly larger than the noise signal occurs at $\delta \leq 40$ km. For the 6-h low-passed trajectories, $\lambda$ is recovered for $\delta \leq 8$ km. For the 12- and 24-h filtering, the lower bound is extended to $\delta \approx 5$ km and $\delta \approx 3$ km, respectively.

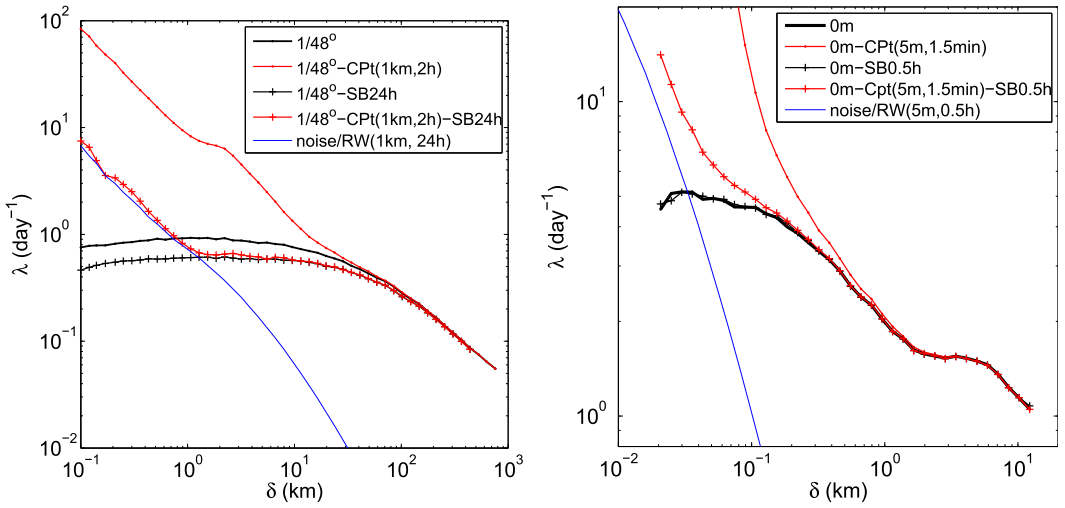


FIG. 11. Adaptive filtering technique in the two models. (left) The HYCOM experiment: FSLE from original and certain HYCOM trajectories with $\Delta t_0 = 2$ h (black line). Measured FSLE signal from uncertain trajectories with $L_K = 1$ km (red line). Signal from observed trajectories subsampled at $\Delta t = 1$ day (red crosses). The FSLE of the (1 km, 1 day) pure random walk (blue line) indicates that the noise is still affecting the signal at scales $\delta < 3$ km. The real signal of the 1-day subsampled trajectories (black crosses) confirms that the FSLE of the filtered real trajectories is recovered for $\delta \geq 3$ km. (right) The LES experiment: the measured signal is the FSLE of the LES trajectories corrupted with a (5 m, 90 s) noise. Similarly, $\Delta t = 30$-min subsampling allows for recovering the 30-min filtered trajectories (almost identical to the real signal) at the scales $\delta \geq 200$ m.

One can see that the adaptive filtering has allowed for a substantial noise extraction and produced an estimate of the drifter-only scale-dependent relative dispersion in the 3–40-km range, although it is a measure of the filtered trajectories. Since the portion of the curve in the transition 7–20 km is robust to the filtering strengths picked in this experiment, we can assume that the features controlling the dispersion at those scales have time scales of at least 1 day and generate substantial cumulative dispersion. For the same reason, they are unlikely related to diurnal oscillations. Term $\lambda$ (3–10 km) of the filtered trajectories are or the order of 1 day$^{-1}$ and about twice the FSLE in the 20–100-km range. The 24-h low-pass filter points to an FSLE plateau at these scales, which would imply an exponential regime set by hyperbolic regions between 5- and 10-km flow features. Note also that the FSLE estimates are similar to HYCOM in winter and fall, which can resolve circulation features up to 4 km. At smaller scales, $\delta < 3$ km, stronger low-pass filters are needed to remove the position uncertainty, but we are limited by the low pair numbers.

## 5. Discussion and summary

As today's oceanic research focuses on small-scale, rapidly evolving flows, Lagrangian observations in the submesoscale range are more prone to aliasing from drifter position uncertainty and sampling frequency. In particular, scale-dependent relative dispersion measurements, which provide information on mixing separately for each spatial scale, require accurate estimates of drifter pair separation velocities. In this study, two sets of synthetic trajectories, one from a high-resolution HYCOM simulation of the North Atlantic circulation and one from a large-eddy simulation of an idealized submesoscale flow field, are used to assess the extent of the noise contribution by corrupting their position with random displacements and to develop a method to recover most of the original signal.

It is found that at scales below the position error standard deviation ($L_K$), the noise generates a mean relative velocity $\langle V \rangle \sim L_K/\Delta t$, where $\Delta t$ is the time interval between two measurements. This results in a $\delta^{-1}$ power-law or spurious ballistic regime, with very high rates of dispersion if either the position uncertainty or the sampling frequency (or both) are significant. For $L_K \approx 1$ km and $\Delta t \approx 1$ h (i.e., SVP drifters), the changes in the rates of dispersion can reach scales up to the radius of deformation, while for $L_K \approx 5$ m and $\Delta t \approx 1$ min (i.e., GPS tracking devices), the increase in $\lambda$ can extend to $O(100\,\text{m})$. Depending on the slope and magnitude of the true FSLE contribution, position errors can impact a range of scales 20–50 times larger than $L_K$. Thus, for a given position uncertainty, a trade-off is required on the sampling frequency to limit the noise signal at the smallest measured scales.

The position error is also found to have a very similar impact as the random walk on the mean relative velocity, while their relative dispersions $D^2(t)$ differ dramatically,

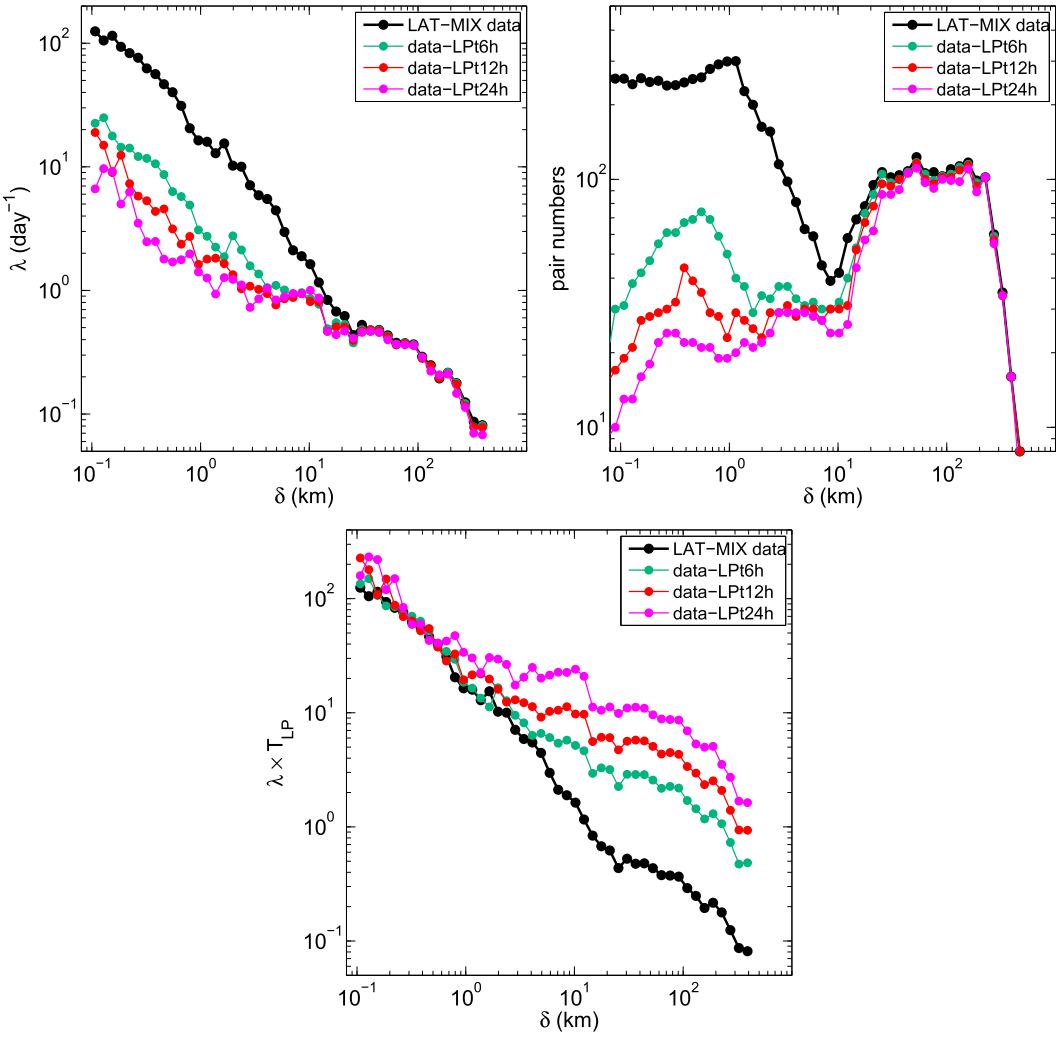


FIG. 12. (top left) Term $\lambda(\delta)$ of the measured and low-passed LatMix June trajectories with time windows $T_{\mathrm{LPt}} = 6$, 12, and 24 h, and minimum pair number of 10. (top right) Corresponding pair number availability. (bottom) Term $\lambda(\delta)$ is rescaled by $1/T_{\mathrm{LPt}}$.

with the position uncertainty generating zero cumulative dispersion. This result implies that the scale-dependent FSLE is more sensitive to pair separation speeds, while $D^2(t)$ is a measure of the time-cumulative dispersion.

Next, the corrupted trajectories are low-pass filtered by either subsampling or a simple time average to reduce the noise contribution. For a noise-dominated signal at $\delta < L_K$, the increase in filter strength is equivalent to an increase in $\Delta t$, which leads to a reduction in the FSLE, since $\lambda$ is linearly dependent on the sampling frequency. On the other hand, the true trajectories contribute to a cumulation of relative dispersion in time and are therefore less sensitive to the low-pass filters. Note that computing $\langle\tau\rangle$ after linearly interpolating the particle positions suppresses the critical $\alpha$ constraint and allows for the use of low sampling frequencies while preserving most of $\lambda(\delta)$. For the HYCOM 1/48° trajectories, the exponential regime is controlled by flow features with time scales of about 1–2 days. Therefore, filtering strengths of less than a 1 day do not affect significantly the exponential regime. For the LES trajectories, the smallest features have time scales of 1–2 h only, such that a 6-h low-pass filter decreases substantially the maximum Lyapunov exponent, including $\lambda$ at the scales of mixed layer instabilities. The degree to which filtered trajectories change $\lambda(\delta)$ appears to be dependent partly on the time scales of the flow features at a given $\delta$ with respect to the filtering time scale $\Delta t$ and partly on their impact on the cumulative relative dispersion. For instance, inertial oscillations will generate less cumulative dispersion than the hyperbolic region between features of the same scales.

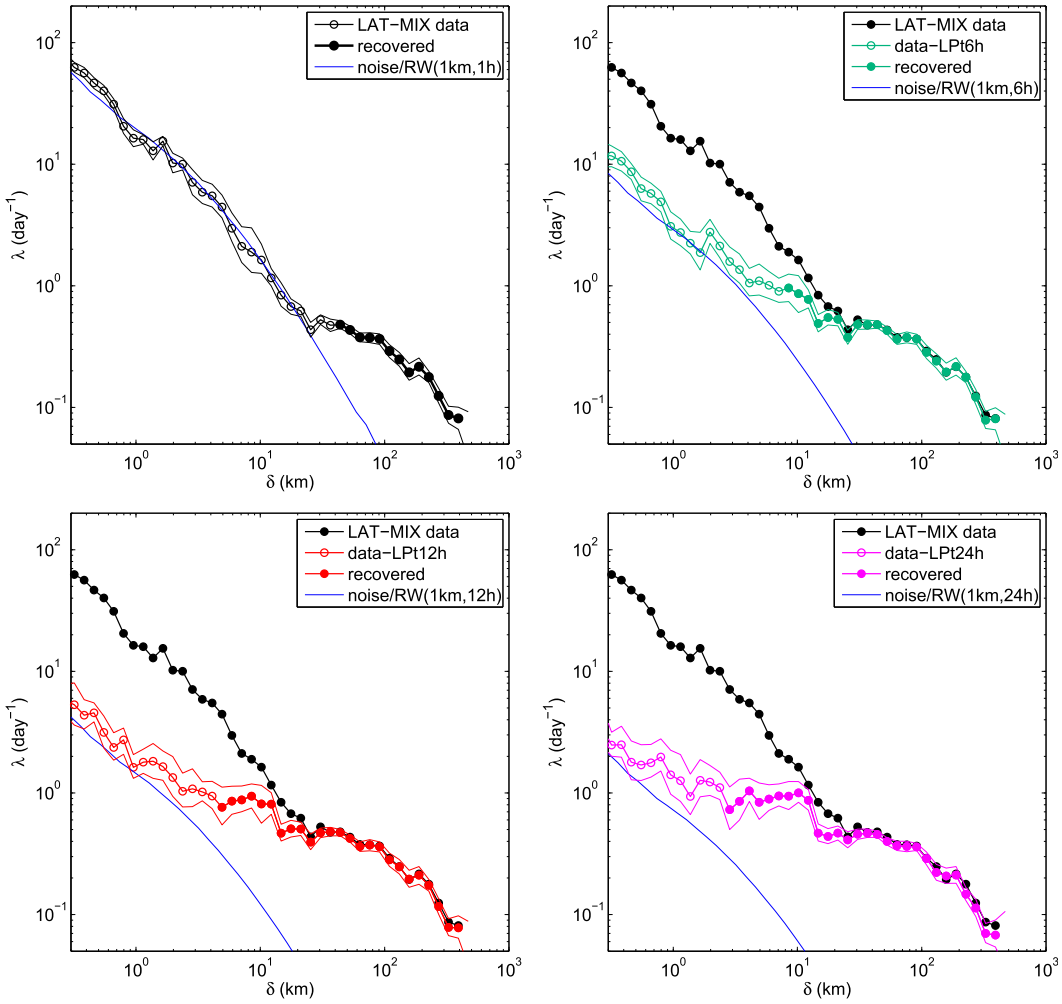


FIG. 13. Term $\lambda(\delta)$ from the raw and low-passed LatMix trajectories with time windows $T_{\mathrm{LPt}} = 6, 12$, and 24 h. Solid line marks the 95% confidence intervals. The random walk FSLE of ($L_K = 1$ km, $\Delta t = T_{\mathrm{LPt}}$) is plotted in blue to illustrate the noise contribution as part of the adaptive filtering. Here $\Delta t = 1$ h for the measured signal. The portion of the recovered signal (i.e., without uncertainty bias) is illustrated by the color-filled circles.

Based on their differing response to low-pass filters, one can recover part of the original signal by gradually increasing the strength of the low-pass filter until the noise contribution becomes negligible with respect to the FSLE of the filtered trajectories. For $\delta \leq L_K$, the position uncertainty FSLE is the same as for a spatially uncorrelated random walk with a turbulent displacement standard deviation of $L_K$ and advection time step $\Delta t$. It remains also quite similar to the random walk FSLE at $\delta > L_K$. It is then possible to use the random walk as reference for the position uncertainty by setting $\Delta t$ to the subsampling time interval or averaging time window. Application of this technique to the synthetic trajectories leads to a recovery of $\lambda$ at scales $\delta > 3$ km for the 1-day filtered HYCOM trajectories and at scales $\delta >$ 200 m for the 30-min filtered LES trajectories. It is possible to further increase the filter strength until the noise is removed at all measured scales. However, it will be done at the expense of the real signal and its information content.

Finally, the adaptive filtering technique is applied to the LatMix drifter dataset. The 20 near-surface SVP drifters were released in pairs in the Gulf Stream in June 2011 to study submesoscale dynamics in summer, and their position uncertainty is of the order of 0.5–1 km. Because of the limited dataset, the scale-dependent relative dispersion is computed from chance pairs and produces a very strong local regime in the submesoscales with values above 10 day$^{-1}$ at scales below 1 km. The drifter trajectories are then low-pass filtered with different time averages $T_{\mathrm{LPt}}$ of 6–24 h, and the collapse of $\lambda$ rescaled by $1/T_{\mathrm{LPt}}$ shows that the FSLE is altered by

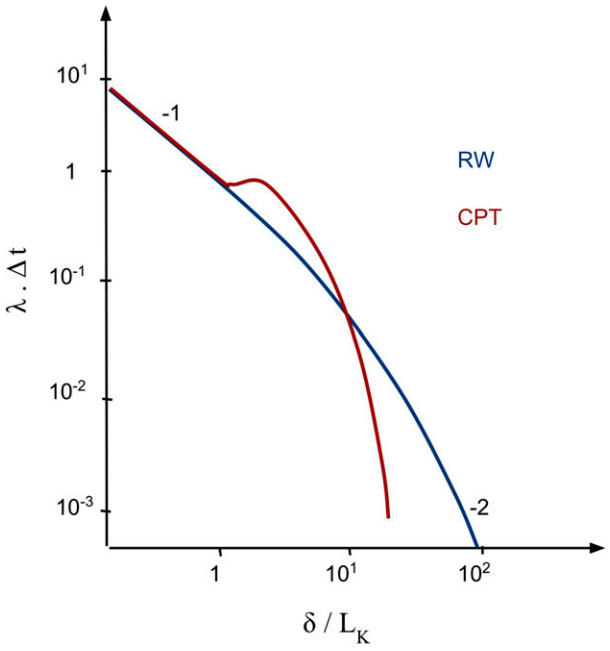


FIG. A1. Schematic diagram depicting the estimated discrepancies in the scale-dependent FSLE between a pure random walk (blue line) and the sole contribution of the position uncertainty (red line). The bump from noise corruption is present at $\delta \approx 1 - 2\,L_K$ and $\lambda_{\mathrm{Cpt}} = \lambda_{\mathrm{RW}}$ at $\delta \approx 10\,L_K$. Then at the scales $\delta \geq 30\,L_K$, $\lambda_{\mathrm{Cpt}}$ is significantly overestimated by $\lambda_{\mathrm{RW}}$.

position uncertainties at scales up to 40 km and dominated by noise at the scales $\delta < 1$ km. The signal is recovered in the 8–40-km range for a 6-h filtering, and in the 3–40-km range for a 1-day filtering (the reduction of available pairs by the low-pass filter at the small scales prevented filtering with a longer time window). Overall, the FSLE estimate of the LatMix drifters appears to have many similarities with the HYCOM 1/48° trajectories, even though the latter ones correspond to the winter season when submesoscales are more prevalent. A jump in the FSLE in the 7–20-km scale range and robustness to the 6–24-h filters indicates time scales of at least 1 day and/or substantial cumulative dispersion. The FSLE of the 1-day filtered trajectories displayed what appears to be a plateau in the 3–10-km range, which would indicate an exponential regime set by 5-km flow features.

Even though a high-resolution OGCM and LES have been used in this study, there needs to be awareness that these models capture only a small range of submesoscale processes, namely, only the mixed layer instability and frontogenesis while relying on various parameterizations and/or simplifications. The ocean is presumably full of submesoscale processes that are not represented here, such as diurnal convection by buoyancy forcing, near-surface shear due to Ekman spiral and near-inertial waves forced by wind, Langmuir turbulence, and Stokes's drift. These processes span a wide range of spatiotemporal scales and their dispersive effects can be recorded by surface drifters. Therefore, we anticipate the demands on the drifter position accuracy to become progressively higher.

In conclusion, the finite-scale Lyapunov exponent is found to be very sensitive to position uncertainty and can be affected in a range of scales extending far beyond the amplitude of the position error. However, the noise signature can be estimated from the standard deviation of the position error measuring device and the sampling frequency, and identified in the FSLE metric. An adaptive filtering technique is developed to remove errors from position uncertainties by taking into account their higher dependence to low-pass filtering. This method allows for recovering much of the information masked by the noise. It also yields valuable information on the time scale of the small-scale features controlling the rate of dispersion, thus providing a more comprehensive picture of the relative dispersion spectrum.

*Acknowledgments.* This study was made possible by grants from the Office of Naval Research and BP/The Gulf of Mexico Research Initiative. The authors would also like to thank two anonymous reviewers for their helpful comments.

## APPENDIX

### FSLE Signal of Position Uncertainty versus Random Walk

The similarities and discrepancies in $\lambda$ for position uncertainty versus random walk are presented in the appendix and illustrated in Fig. A1.

The scale-dependent FSLE of the position uncertainty $\lambda_{\mathrm{Cpt}}$ at scales $\delta < L_K$ can be approximated by the expression defined in Eq. (14) and is the same as for a pure random walk. At scales $L_K < \delta < 3\,L_K$, $\lambda_{\mathrm{Cpt}}$ displays a "bump" characteristic of the noise amplitude $L_K$. It is visible in both sets of synthetic trajectories and remains unaffected by subsampling.

The bump corresponds also to the maximum scale $\delta \approx 2\,L_K$ for which $\lambda_{\mathrm{Cpt}}$ can be computed directly from particle pairs at a fixed location with a position uncertainty of $(L_K, \Delta t)$. Beyond this scale, $\lambda_{\mathrm{Cpt}}$ can only be estimated empirically from different experiments of the synthetic HYCOM and LatMix LES trajectories. For $L_K < \delta < 10\,L_K$, $\lambda_{\mathrm{Cpt}}$ is slightly underestimated by $\lambda_{\mathrm{RW}}$, partly due to the presence of the bump. For the range of scales $\delta > 30\,L_K$, $\lambda_{\mathrm{Cpt}}$ becomes overestimated by $\lambda_{\mathrm{RW}}$.

In the range $\delta > 2L_K$, extracting the noise contribution from the real signal requires the use of excessively high $L_K$s and sampling frequencies, which is not realistic. In a normal ocean setting, there is more likely a combination of noise and real relative dispersion speeds, so that the noise FSLE depicted in Fig. A1 is only a guess. For this reason, it is preferable to use the FSLE of the pure random walk ($\lambda_{RW}$) as a reference for the noise contribution at all spatial scales below 30 $L_K$.

## REFERENCES


Artale, V., G. Boffetta, A. Celani, M. Cencini, and A. Vulpiani, 1997: Dispersion of passive tracers in closed basins: Beyond the diffusion coefficient. *Phys. Fluids,* **9,** 3162–3171, doi:10.1063/1.869433.

Aurell, E., G. Boffetta, A. Crisanti, G. Paladin, and A. Vulpiani, 1997: Predictability in the large: An extension of the concept of Lyapunov exponent. *J. Phys.,* **30A,** doi:10.1088/0305-4470/30/1/003.

Babiano, A., C. Basdevant, P. Le Roy, and R. Sadourny, 1990: Relative dispersion in two-dimensional turbulence. *J. Fluid Mech.,* **214,** 535–557, doi:10.1017/S0022112090000258.

Badin, G., A. Tandon, and A. Mahadevan, 2011: Lateral mixing in the pycnocline by baroclinic mixed layer eddies. *J. Phys. Oceanogr.,* **41,** 2080–2101, doi:10.1175/JPO-D-11-05.1.

Batchelor, G. K., 1952: Diffusion in a field of homogeneous turbulence. II. The relative motion of particles. *Math. Proc. Cambridge Philos. Soc.,* **48,** 345–362, doi:10.1017/S0305004100027687.

Bennett, A. F., 1984: Relative dispersion: Local and nonlocal dynamics. *J. Atmos. Sci.,* **41,** 1881–1886, doi:10.1175/1520-0469(1984)041<1881:RDLAND>2.0.CO;2.

Berti, S., F. A. D. Santos, G. Lacorata, and A. Vulpiani, 2011: Lagrangian drifter dispersion in the southwestern Atlantic Ocean. *J. Phys. Oceanogr.,* **41,** 1659–1672, doi:10.1175/2011JPO4541.1.

Boccaletti, G., R. Ferrari, and B. Fox-Kemper, 2007: Mixed layer instabilities and restratification. *J. Phys. Oceanogr.,* **37,** 2228–2250, doi:10.1175/JPO3101.1.

Boffetta, G., A. Celani, M. Cencini, G. Lacorata, and A. Vulpiani, 2000: Nonasymptotic properties of transport and mixing. *Chaos,* **10,** 50, doi:10.1063/1.166475.

Capet, X., J. McWilliams, M. Molemaker, and A. Shchepetkin, 2008: Mesoscale to submesoscale transition in the California Current System. Part I: Flow structure, eddy flux, and observational tests. *J. Phys. Oceanogr.,* **38,** 29–43, doi:10.1175/2007JPO3671.1.

Carrier, M., H. Ngodock, S. Smith, P. Muscarella, G. Jacobs, T. Özgökmen, B. Haus, and B. Lipphardt, 2014: Impact of ocean velocity observations inferred from Lagrangian drifter data using the NCOM-4DVAR. *Mon. Wea. Rev.,* **142,** 1509–1524, doi:10.1175/MWR-D-13-00236.1.

Chassignet, E., H. Hurlburt, O. Smedstad, G. Halliwell, P. Hogan, A. Wallcraft, and R. Bleck, 2006: Ocean prediction with the Hybrid Coordinate Ocean Model (HYCOM). *Ocean Wea. Forecasting,* **5,** 413–426, doi:10.1007/1-4020-4028-8_16.

Fox-Kemper, B., R. Ferrari, and R. Hallberg, 2008: Parameterization of mixed-layer eddies. Part I: Theory and diagnosis. *J. Phys. Oceanogr.,* **38,** 1145–1165, doi:10.1175/2007JPO3792.1.

Hansen, D. V., and P. M. Poulain, 1996: Quality control and interpolations of WOCE-TOGA drifter data. *J. Atmos. Oceanic Technol.,* **13,** 900–909, doi:10.1175/1520-0426(1996)013<0900:QCAIOW>2.0.CO;2.

Haza, A. C., A. Poje, T. M. Özgökmen, and P. Martin, 2008: Relative dispersion from a high-resolution coastal model of the Adriatic Sea. *Ocean Modell.,* **22,** 48–65, doi:10.1016/j.ocemod.2008.01.006.

——, T. M. Özgökmen, A. Griffa, Z. D. Garraffo, and L. I. Piterbarg, 2012: Parametrization of particle transport at submesoscales in the Gulf Stream region using Lagrangian subgridscale models. *Ocean Modell.,* **42,** 31–49, doi:10.1016/j.ocemod.2011.11.005.

Kirwan, A. D. J., and M. S. Chang, 1979: Effect of sampling rate and random position error on analysis of drifter data. *J. Phys. Oceanogr.,* **9,** 382–387, doi:10.1175/1520-0485(1979)009<0382:EOSRAR>2.0.CO;2.

Klein, P., and G. Lapeyre, 2009: The oceanic vertical pump induced by mesoscale and submesoscale turbulence. *Annu. Rev. Mar. Sci.,* **1,** 351–375, doi:10.1146/annurev.marine.010908.163704.

Koszalka, I., J. H. LaCasce, and K. A. Orvik, 2009: Relative dispersion statistics in the Nordic Seas. *J. Mar. Res.,* **67,** 411–433, doi:10.1357/002224009790741102.

LaCasce, J. H., 2008: Statistics from Lagrangian observations. *Prog. Oceanogr.,* **77,** 1–29, doi:10.1016/j.pocean.2008.02.002.

——, and C. Ohlmann, 2003: Relative dispersion at the surface of the Gulf of Mexico. *J. Mar. Res.,* **61,** 285–312, doi:10.1357/002224003322201205.

Lacorata, G., E. Aurell, and A. Vulpiani, 2001: Drifter dispersion in the Adriatic Sea: Lagrangian data and chaotic model. *Ann. Geophys.,* **19,** 121–129, doi:10.5194/angeo-19-121-2001.

Lumpkin, R., and M. Pazos, 2007: Measuring surface currents with Surface Velocity Program drifters: The instrument, its data, and some recent results. *Lagrangian Analysis and Prediction of Coastal and Ocean Dynamics,* A. Griffa et al., Eds., Cambridge University Press, 39–67.

——, and S. Elipot, 2010: Surface drifter pair spreading in the North Atlantic. *J. Geophys. Res.,* **115,** C12017, doi:10.1029/2010JC006338.

Mahadevan, A., and A. Tandon, 2006: An analysis of mechanisms for submesoscale vertical motion at ocean fronts. *Ocean Modell.,* **14,** 241–256, doi:10.1016/j.ocemod.2006.05.006.

McWilliams, J., 2008: Fluid dynamics at the margin of rotational control. *Environ. Fluid Mech.,* **8,** 441–449, doi:10.1007/s10652-008-9081-8.

Mensa, J., A. Griffa, Z. Garraffo, T. Özgökmen, A. Haza, and M. Veneziani, 2013: Seasonality of the submesoscale dynamics in the Gulf Stream region. *Ocean Dyn.,* **63,** 923–941, doi:10.1007/s10236-013-0633-1.

Müller, P., J. McWilliams, and M. Molemaker, 2005: Routes to dissipation in the ocean: The two-dimensional/three-dimensional turbulence conundrum. *Marine Turbulence: Theories, Observations, and Models; Results of the CARTUM Project,* H. Z. Baumert, J. Simpson, and J. Sündermann, Eds., Cambridge University Press, 397–405.

Ohlmann, J. C., P. F. White, A. L. Sybrandy, and P. P. Niiler, 2005: GPS–cellular drifter technology for coastal ocean observing system. *J. Atmos. Oceanic Technol.,* **22,** 1381–1388, doi:10.1175/JTECH1786.1.

Olascoaga, M. J., and Coauthors, 2013: Drifter motion in the Gulf of Mexico constrained by altimetric Lagrangian coherent structures. *Geophys. Res. Lett.,* **40,** 6171–6175, doi:10.1002/2013GL058624.

Özgökmen, T., and P. Fischer, 2012: CFD application to oceanic mixed layer sampling with Lagrangian platforms. *Int. J. Comput. Fluid Dyn.,* **26,** 337–348, doi:10.1080/10618562.2012.668888.

——, A. Poje, P. Fischer, and A. Haza, 2011: Large eddy simulations of mixed layer instabilities and sampling strategies. *Ocean Modell.,* **39,** 311–331, doi:10.1016/j.ocemod.2011.05.006.

——, ——, ——, H. Childs, H. Krishnan, C. Garth, A. Haza, and E. Ryan, 2012: On multi-scale dispersion under the influence of surface mixed layer instabilities and deep flows. *Ocean Modell.,* **56,** 16–30, doi:10.1016/j.ocemod.2012.07.004.

Piterbarg, L., 2012: Finite size Lyapunov exponent for some simple models of turbulence. *Appl. Math. Modell.,* **36,** 3464–3476, doi:10.1016/j.apm.2011.10.024.

Poje, A., A. Haza, T. Özgökmen, M. Magaldi, and Z. Garraffo, 2010: Resolution dependent relative dispersion statistics in a hierarchy of ocean models. *Ocean Modell.,* **31,** 36–50, doi:10.1016/j.ocemod.2009.09.002.

——, and Coauthors, 2014: Submesoscale dispersion in the vicinity of the *Deepwater Horizon* Oil Spill. *Proc. Natl. Acad. Sci. USA,* **111,** 12 693–12 698, doi:10.1073/pnas.1402452111.

Richardson, L. F., 1926: Atmospheric diffusion shown on a distance-neighbour graph. *Proc. Roy. Soc. London,* **110A,** 709–737, doi:10.1098/rspa.1926.0043.

Schroeder, K., A. C. Haza, A. Griffa, T. M. Özgökmen, P. Poulain, R. Gerin, G. Peggion, and M. Rixen, 2011: Relative dispersion in the Liguro-Provençal basin: From sub-mesoscale to mesoscale. *Deep-Sea Res. I,* **58,** 209–228, doi:10.1016/j.dsr.2010.11.004.

——, and Coauthors, 2012: Targeted Lagrangian sampling of submesoscale dispersion at a coastal frontal zone. *Geophys. Res. Lett.,* **39,** L11608, doi:10.1029/2012GL051879.

Shcherbina, A., E. A. D. Asaro, C. M. Lee, J. M. Klymak, M. J. Molemaker, and J. C. McWilliams, 2013: Statistics of vertical vorticity, divergence, and strain in a developed submesoscale turbulence field. *Geophys. Res. Lett.,* **40,** 4706–4711, doi:10.1002/grl.50919.

Thomas, L., A. Tandon, and A. Mahadevan, 2008: Submesoscale processes and dynamics. *Ocean Modeling in an Eddying Regime, Geophys. Monogr.,* Vol. 177, Amer. Geophys. Union, 17–38.

Zhong, Y., A. Bracco, and T. Villareal, 2012: Pattern formation at the ocean surface: Sargassum distribution and the role of the eddy field. *Limnol. Oceanogr. Fluids Environ.,* **2,** 12–27, doi:10.1215/21573689-1573372.